Laplace wavelet transform theory and applications

Article *in* Journal of Vibration and Control · May 2017

DOI: 10.1177/1077546317707103

CITATIONS
13

READS
2,594

3 authors:

Tariq Abuhamdia
KLA Corporation
5 PUBLICATIONS **37** CITATIONS
SEE PROFILE

Saied Taheri
Virginia Tech (Virginia Polytechnic Institute and State University)
132 PUBLICATIONS **2,243** CITATIONS
SEE PROFILE

John A. Burns
Virginia Tech (Virginia Polytechnic Institute and State University)
189 PUBLICATIONS **3,308** CITATIONS
SEE PROFILE

Review

Journal of Vibration and Control
1–21

DOI: 10.1177/1077546317707103
journals.sagepub.com/home/jvc
SAGE

Laplace wavelet transform theory and applications

Tariq Abuhamdia[1], Saied Taheri[1] and John Burns[2]

Abstract

This study introduces the theory of the Laplace wavelet transform (LWT). The Laplace wavelets are a generalization of the second-order under damped linear time-invariant (SOULTI) wavelets to the complex domain. This generalization produces the mother wavelet function that has been used as the Laplace pseudo wavelet or the Laplace wavelet dictionary. The study shows that the Laplace wavelet can be used to transform signals to the time-scale or time-frequency domain and can be retrieved back. The properties of the new generalization are outlined, and the characteristics of the companion wavelet transform are defined. Moreover, some similarities between the Laplace wavelet transform and the Laplace transform arise, where a relation between the Laplace wavelet transform and the Laplace transform is derived. This relation can be beneficial in evaluating the wavelet transform. The new wavelet transform has phase and magnitude, and can also be evaluated for most elementary signals. The Laplace wavelets inherit many properties from the SOULTI wavelets, and the Laplace wavelet transform inherits many properties from both the SOULTI wavelet transform and the Laplace transform. In addition, the investigation shows that both the LWT and the SOULTI wavelet transform give the particular solutions of specific related differential equations, and the particular solution of these linear time-invariant differential equations can in general be written in terms of a wavelet transform. Finally, the properties of the Laplace wavelet are verified by applications to frequency varying signals and to vibrations of mechanical systems for modes decoupling, and the results are compared with the generalized Morse and Morlet wavelets in addition to the short time Fourier transform's results.

Keywords

Chirp analysis, complex wavelets, frequency-identification, Laplace wavelets, mode decoupling, particular solution, second-order systems wavelets, scalogram, spectrogram, time-frequency analysis, transform

1. Introduction

The applications of wavelets have developed significantly in recent years, especially in systems analysis. The applications of wavelets as a tool for analyzing signals have been extended to analyze systems and their mathematical models.

The applications of wavelets in systems and control include response solution, system identification, system representation, and control design. For a comprehensive review on wavelets use in systems and control we refer the reader to Abuhamdia and Taheri (2015). The suitability of a wavelet function to analyze a system depends on the similarity between the wavelet properties and response function of the system. Consequently, the second-order under damped linear time-invariant (SOULTI) wavelets (Abuhamdia et al., 2016) provide a suitable tool to investigate the linearity of vibratory systems and to find their characteristics because they are derived from the response of second-order underdamped linear time-invariant (LTI) systems.

The introduction of the SOULTI wavelets (Abuhamdia et al., 2016) gave many advantages to wavelets analysis of systems and signals. For example, the wavelet transform can be evaluated and formulas can be obtained for the wavelet transformation of most

[1]Center for Tire Research (CenTire), Virginia Polytechnic Institute and State University, USA
[2]Interdisciplinary Center for Applied Mathematics (ICAM), Virginia Polytechnic Institute and State University, USA

Received: 2 October 2016; accepted: 3 April 2017

Corresponding author:
Tariq Abuhamdia, Department of Mechanical Engineering, Virginia Tech, 100T Randolph Hall, 460 Old Turner St, Blacksburg, VA, 24060, USA.
Email: atariqm@vt.edu

elementary signals. There exists direct relation between the frequency and the scale, and an algebraic formula can be used to find the inverse wavelet transform. The SOULTI wavelet is a real function, and the corresponding wavelet transform is real.

Generalizing the SOULTI wavelets to the complex domain produces the Laplace wavelet, which introduces an additional cosine component. This introduction yields magnitude and phase for the transform, which gives more insight into the change of periodicity of the signal and the change of the complex phase. Moreover, the resulting wavelet becomes similar to the Laplace transform kernel, which is another advantage because the Laplace transform is easy to evaluate and can be used to find systems' dynamic properties.

Laplace wavelets are not new. They were first introduced in the work of Freudinger et al. (1998). However, they were used as pseudo wavelets that form a dictionary but not basis or frame. Moreover, the inverse of the Laplace wavelet transform was not investigated. So, to date, the use and capability of the Laplace wavelets remained limited. Another close approach was the Cauchy wavelets introduced by (Jezequel and Argoul, 1986). They used functions in the frequency domain as wavelets or transform kernels. These functions represent transfer functions of first- or higher-order LTI systems.

The relationship between the Laplace wavelet and the SOULTI wavelet is direct, where the SOULTI wavelet is the imaginary part of the Laplace wavelet, while the real part is an exponentially decaying sinusoidal function but with a cosine term. The next section draws a natural derivation of the Laplace wavelets and shows the relationship between the Laplace wavelet transform (LWT) and the Laplace transform. Section 3 presents the inverse Laplace wavelet transform (ILWT) and its relations to the particular solution of LTI differential equations, while Section 4 introduces the LWT for basic elementary signals and some properties of the transform. In Section 5 we verify the potentials of the LWT by applying it to oscillatory signals and a vibrational system response. It is important to note that the terms "autonomous" and "time-invariant" are used interchangeably to describe differential equations. "Time-invariant" is usually used in the context of dynamic systems, whereas "autonomous" is usually used in mathematical contexts.

2. Generalizing the SOULTI wavelet (the Laplace wavelet)

The SOULTI wavelet is derived from the response of second-order underdamped LTI systems, hence the name (Abuhamdia et al., 2016). The wavelet SOULTI, which is a real wavelet, is defined by

$$\psi_{\zeta}^{a,\tau} = \psi_{\zeta}\left(\frac{t-\tau}{a}\right) = \left(\frac{a^{-p}}{1-\zeta^2}\right) e^{\frac{-\zeta}{\sqrt{1-\zeta^2}}\left(\frac{t-\tau}{a}\right)} \times \sin\left(\frac{t-\tau}{a}\right) u(t-\tau) \tag{1}$$

where $0 < \zeta < 1$ specifies the wavelet family, τ is the time-shifting variable, $a > 0$ is the scaling variable, $u(t)$ is the Heaviside step function, and p is a property preserving parameter, which takes the values of 1 or $\frac{1}{2}$. The L^1, L^2 integration of the wavelet is preserved constant for $p = 1$, $p = \frac{1}{2}$ respectively, where ζ is held fixed.

Let us introduce the decaying cosine function as

$$\left(\frac{a^{-p}}{1-\zeta^2}\right) e^{\frac{-\zeta}{\sqrt{1-\zeta^2}}\left(\frac{t-\tau}{a}\right)} \cos\left(\frac{t-\tau}{a}\right) u(t-\tau) \tag{2}$$

which resembles the real part of the Laplace wavelet, $Re(\psi_{L_\zeta}^{a,\tau})$. If we let the SOULTI wavelet in equation (1) be the imaginary part and let the function in equation (2) be the real part, then we can define the Laplace wavelet as

$$\psi_{L_\zeta}^{a,\tau} = \left(\frac{a^{-p}}{1-\zeta^2}\right) e^{\frac{-\zeta}{\sqrt{1-\zeta^2}}\left(\frac{t-\tau}{a}\right)} \cos\left(\frac{t-\tau}{a}\right) u(t-\tau) + j\left(\frac{a^{-p}}{1-\zeta^2}\right) e^{\frac{-\zeta}{\sqrt{1-\zeta^2}}\left(\frac{t-\tau}{a}\right)} \sin\left(\frac{t-\tau}{a}\right) u(t-\tau) \tag{3}$$

where $j = \sqrt{-1}$. Using Euler formula, the definition in equation (3) can be rewritten in compact form as

$$\psi_{L_\zeta}^{a,\tau} = \left(\frac{a^{-p}}{1-\zeta^2}\right) e^{\left(\frac{-\zeta}{\sqrt{1-\zeta^2}}+j\right)\left(\frac{t-\tau}{a}\right)} u(t-\tau) \tag{4}$$

Figure 1 shows a plot of the Laplace wavelet. In general, the Laplace wavelet defined in equation (4)

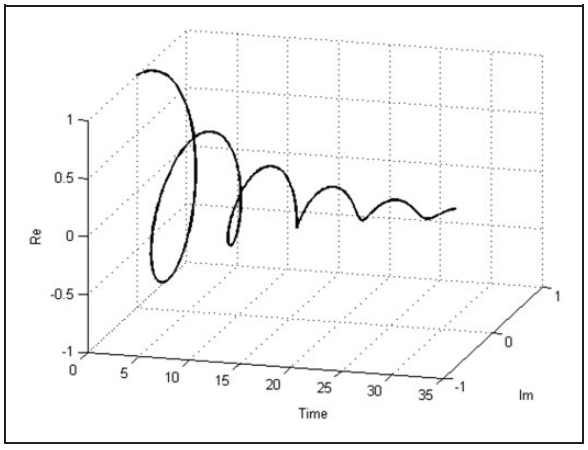

Figure 1. The Laplace wavelet.

does not satisfy $< \psi_{L_{\zeta_r}}^{a_v,\tau}, \psi_{L_{\zeta_q}}^{a_w,\tau} > = \delta_{r,q,w,v}$, where $\delta_{r,q,w,v} = 1$ if $r = q = u = v$ and 0 otherwise. However, the Laplace wavelet function in equation (4) is orthogonal to

$$\psi_{L_\zeta}^{a,\tau} = \left(\frac{a^{-p}}{1-\zeta^2}\right) e^{\left(\frac{\zeta}{\sqrt{1-\zeta^2}}+j\right)\left(\frac{t-\tau}{a}\right)} u(t-\tau) \tag{5}$$

2.1. The Laplace transform and the Laplace wavelet transform

Suppose that $J \subset (a,\infty) \subset \mathbb{R}$, and let $f(t) : J \to \mathbb{R}$, where $f(t) \in L^1$ and is exponentially bounded, see Definition 3.1, then using the definition of the Laplace wavelet in equation (4), the LWT of $f(t)$ reads

$$\begin{aligned} \tilde{f}_{L_\zeta}(\tau,a) = \mathcal{W}_{L_\zeta}\{f(t)\} &= < \psi_{L\zeta}^{a,\tau}, f(t) > \\ &= \left(\frac{a^{-p}}{1-\zeta^2}\right) \int_\tau^\infty \overline{e^{\left(\frac{-\zeta}{\sqrt{1-\zeta^2}}+j\right)\left(\frac{t-\tau}{a}\right)}} f(t)\mathrm{d}t \end{aligned} \tag{6}$$

Where the over-bar signifies the complex conjugate. Now, we can establish a relation between the Laplace transform and the LWT. The Laplace transform is defined as

$$\mathcal{L}\{f(t)\} = F(s) = \int_{-\infty}^{\infty} e^{-st} f(t)\mathrm{d}t \tag{7}$$

which can be written for right-sided signals, namely $f(t) = 0$ if $t < 0$, as

$$F(s) = \int_0^\infty e^{-st} f(t)\mathrm{d}t \tag{8}$$

where $s \in \mathbb{C}$ is the Laplace complex variable. Now, consider the exponent part in equation (6) and make the substitutions

$$\sigma = \frac{1}{a}\left(\frac{\zeta}{\sqrt{1-\zeta^2}} + j\right) \tag{9}$$

$$c = \left(\frac{1}{1-\zeta^2}\right) \tag{10}$$

then substitute equations (9) and (10) back into equation (6) to arrive at

$$\tilde{f}_{L_\zeta}(\tau,\sigma) = ca^{-p} \int_\tau^\infty e^{-\sigma(t-\tau)} f(t)\mathrm{d}t \tag{11}$$

Because $u(t-\tau) = 0$, $t \le \tau$, the integration lower limit changed to start from τ, and the Heaviside function is dropped from the integration. By comparing equations (8) and (11), we find that the Laplace wavelet transform is similar to the Laplace transform with positive time-delay, namely $\mathcal{L}\{f(t+\tau)\}$, but the lower limit of the integration is different. However, the time-shifting property of the Laplace transform does not apply here, because the Laplace wavelet, which is the transform kernel, is right-sided. When the kernel is right-sided and a positive shift is applied to the transformed signal, part of the signal becomes multiplied by zero and does not count for the integration. In this case, the Laplace time-shifting property is only applicable when the shift is negative.

Alternatively, the Laplace wavelet transform in equation (11), can be written as

$$\tilde{f}_{L_\zeta}(\tau,\sigma) = ca^{-p} e^{\sigma\tau} \int_\tau^\infty e^{-\sigma t} f(t)\mathrm{d}t \tag{12}$$

which can be split into two parts as

$$\tilde{f}_{L_\zeta}(\tau,\sigma) = ca^{-p} e^{\sigma\tau} \left(\int_0^\infty e^{-\sigma t} f(t)\mathrm{d}t - \int_0^\tau e^{-\sigma t} f(t)\mathrm{d}t \right) \tag{13}$$

where the first term inside the parenthesis is the Laplace transform of $f(t)$, so equation (13) can be written as

$$\mathcal{W}_{L_\zeta}\{f(t)\} = ca^{-p} e^{\sigma\tau} \left(\mathcal{L}\{f(t)\}|_{s=\sigma} - \int_0^\tau e^{-\sigma t} f(t)\mathrm{d}t \right) \tag{14}$$

Equation (14) shows the relation between the Laplace transform and the LWT. It is important to notice that with the LWT not all the complex Laplace domain is covered. The transform is only restricted to the region in the complex domain determined by equation (9). Figure 2 shows the relationship between the Laplace domain and the time-scale domain of the LWT. The time-scale domain intersects perpendicularly the Laplace domain, where the time axis is perpendicular to the Laplace complex plane. Each ray that emerges from the origin in the left half plane represents a Laplace wavelet family. Each wavelet family is determined by the parameter ζ, which is restricted to the range $0 < \zeta < 1$. The parameter ζ controls the angle between the scale axis and the real axis of the Laplace domain, where the angle is given by

$$\phi(\zeta) = \tan^{-1}\left(\frac{\zeta}{\sqrt{1-\zeta^2}}\right) = \cos^{-1}(\zeta) \tag{15}$$

Also, note that the permissible range of σ on the Laplace domain includes the left half-plane except the real and imaginary axes.

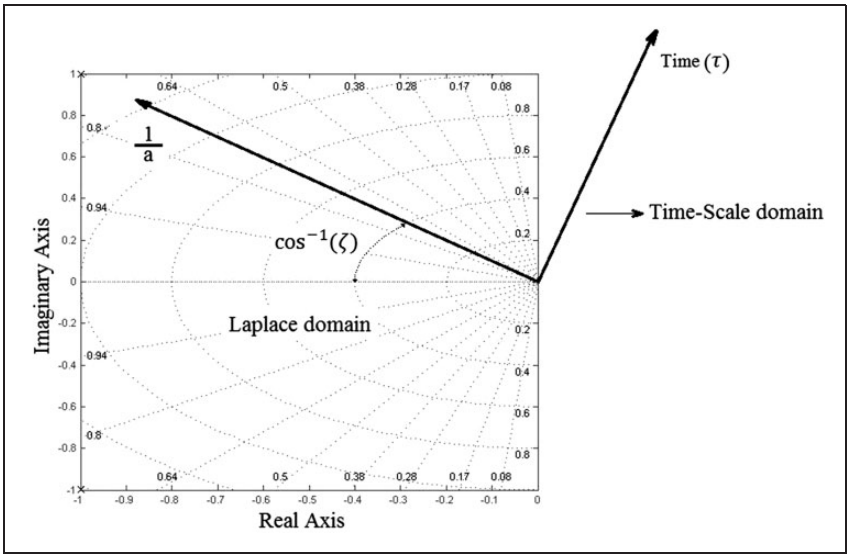

Figure 2. The Laplace domain and the time-scale domain.

The transform in equation (6) can be evaluated either by direct substitution of the signal into the integral or by evaluating the real and imaginary parts separately and then combining the two together. Also, we can use the similarity between the Laplace transform and the Laplace wavelet transform to evaluate the LWT.

3. Inverse Laplace wavelet transform

Evaluating the inverse Laplace wavelet transform (ILWT) is similar to evaluating the inverse SOULTI wavelet transform, and deriving the inverse formula is parallel to deriving the inverse formula of the SOULTI wavelet transform (Abuhamdia et al., 2016). Moreover, for simple signals, the real part of the Laplace wavelet transform can be used directly to evaluate the ILWT by applying the Inverse SOULTI wavelet transform to the imaginary part of the LWT.

The Fourier transform of the Laplace mother wavelet is given by

$$\begin{aligned}\mathcal{F}\{\psi_{L_\zeta}(t)\} &= \mathcal{F}\left\{\frac{a^{-p}}{1-\zeta^2}e^{\left(\frac{-\zeta}{\sqrt{1-\zeta^2}}+j\right)t}\right\} \\ &= \frac{a^{-p}}{j(1-\zeta^2)(\omega-1)+\zeta\sqrt{1-\zeta^2}}\end{aligned} \tag{16}$$

For a shifted and scaled version of the wavelet, the Fourier transform is given by

$$\begin{aligned}\mathcal{F}\left\{\psi_{L_\zeta}\left(\frac{t-\tau}{a}\right)\right\} &= ae^{-j\omega\tau}\Psi_{L_\zeta}(a\omega) \\ &= e^{-j\omega\tau}\frac{a^{1-p}}{j(1-\zeta^2)(a\omega-1)+\zeta\sqrt{1-\zeta^2}}\end{aligned} \tag{17}$$

since $a>0$, then $\Psi_{L_\zeta}(a\omega)$ never vanishes. Using the Plancherel's identity (Yoshida, 1965), the Fourier transform of $f(t)$ becomes

$$\tilde{f}_{L_\zeta}(\tau,a)=\frac{a}{2\pi}\int_{-\infty}^{\infty}e^{j\omega\tau}\overline{\Psi_{L_\zeta}(a\omega)}F(\omega)\mathrm{d}\omega \tag{18}$$

Equation (18) is equal to the inverse Fourier transform of $a\overline{\Psi_{L_\zeta}(a\omega)}F(\omega)$, where $\overline{\Psi_{L_\zeta}(a\omega)}$ is the complex conjugate of $\Psi_{L_\zeta}(a\omega)$. By applying the Fourier transform to both sides of equation (18), we arrive at

$$\int_{-\infty}^{\infty}e^{-j\omega\tau}\tilde{f}_{L_\zeta}(\tau,a)\mathrm{d}\tau=a\overline{\Psi_{L_\zeta}(a\omega)}F(\omega) \tag{19}$$

Dividing by $\overline{\Psi_{L_\zeta}(a\omega)}$ is a legitimate operation since it does not vanish for any value of ω or a. When equation (19) is solved for $F(\omega)$, we obtain

$$F(\omega)=\frac{1}{a\overline{\Psi_{L_\zeta}(a\omega)}}\int_{-\infty}^{\infty}e^{-j\omega\tau}\tilde{f}_{L_\zeta}(\tau,a)\mathrm{d}\tau \tag{20}$$

Applying the inverse Fourier transform to both sides of equation (20) retrieves $f(t)$ back in the form

$$f(t)=\frac{1}{2\pi}\int_{-\infty}^{\infty}\int_{-\infty}^{\infty}\frac{1}{a\overline{\Psi_{L_\zeta}(a\omega)}}e^{-j\omega(\tau-t)}\tilde{f}_{L_\zeta}(\tau,a)\mathrm{d}\tau\mathrm{d}\omega \tag{21}$$

Equation (21) represents an integral formula for the ILWT. In the following, we show that other formulas are possible if $f(t)$ satisfies certain conditions.

3.1. Definition: exponential boundedness

Define $J \subset (a, \infty) \subset \mathbb{R}$, and let $f(t) : J \to \mathbb{R}$, if $\exists\, \alpha$ and $k \in \mathbb{R}$ such that $|f(t)| \leq |k.e^{\alpha t}| \forall t \in J$, then $f(t)$ is exponentially bounded. Now, some theorems and corollaries can be introduced in a parallel approach to the SOULTI wavelet theorems (Abuhamdia et al., 2016).

3.2. Theorem: Inverse Laplace wavelet transform

Let $J \subset (\alpha, \infty) \subset \mathbb{R}$, and let $f(t) : J \to \mathbb{R}$ be integrable and exponentially bounded, and let the Laplace wavelet transform of $f(t)$ be given by equation (6), then $f(t)$ can be retrieved back from its wavelet transform $\tilde{f}_{L_\zeta}(t, a)$, using the identity

$$f(t) = a^{p-1}\left(-(1-\zeta^2)a\frac{\mathrm{d}\left(\tilde{f}_{L_\zeta}(t,a)\right)}{\mathrm{d}t} + \left(j(1-\zeta^2) + \zeta\sqrt{1-\zeta^2}\right)\tilde{f}_{L_\zeta}(t,a)\right) \tag{22}$$

Proof. Substituting $a\overline{\Psi_\zeta(a\omega)}$ from equation (17) into equation (21) gives

$$f(t) = \int_{-\infty}^{\infty} \frac{e^{j\omega t}}{2\pi a^{1-p}}\left(j(1-\zeta^2)(1-a\omega) + \zeta\sqrt{1-\zeta^2}\right) \times \int_{-\infty}^{\infty} e^{-j\omega t}\tilde{f}_{L_\zeta}(t,a)\mathrm{d}t\,\mathrm{d}\omega \tag{23}$$

Using the operator notation for the Fourier transform, equation (23) becomes

$$f(t) = a^{p-1}\mathcal{F}^{-1}\left\{\left(-j(1-\zeta^2)a\omega + j(1-\zeta^2) + \zeta\sqrt{1-\zeta^2}\right) \times \mathcal{F}\left\{\tilde{f}_{L_\zeta}(t,a)\right\}\right\} \tag{24}$$

Applying the linear operators' properties (Naylor and Sell, 2000) to equation (24) gives

$$f(t) = a^{p-1}\mathcal{F}^{-1}\left\{-j(1-\zeta^2)a\omega\mathcal{F}\left\{\tilde{f}_{L_\zeta}(t,a)\right\}\right\} + a^{p-1}\mathcal{F}^{-1}\left\{\left(j(1-\zeta^2) + \zeta\sqrt{1-\zeta^2}\right)\mathcal{F}\left\{\tilde{f}_{L_\zeta}(t,a)\right\}\right\} \tag{25}$$

and after applying the Fourier transform differentiation property to equation (25) we arrive at equation (22). ■

This result parallels a similar result for the SOULTI wavelet (Abuhamdia et al., 2016). However, the requirement on $\tilde{f}_{L_\zeta}(\tau, a)$ is to be differentiable, which is satisfied if $f(t)$ is integrable and exponentially bounded.

Theorem 3.2 proves that $\tilde{f}_\zeta$ is a solution of equation (22). However, by observing Table 1 we find that the solution given by the wavelet transform is the particular solution. By plugging each of the basic functions in Table 1 in equation (22) and solving for the particular solution using the method of undetermined coefficients, it can be demonstrated that the LWT gives the particular solution for that specific function.

In the following we provide a proof showing that the LWT gives the particular solution of first-order linear autonomous differential equations with positive characteristic equation root. In other words, the particular solution given by the variation of parameters method is a wavelet transform.

3.3. Theorem: particular solution by wavelet transform

Let $J \subset (\lambda, \infty) \subset \mathbb{R}$, and let $f(t) : J \to \mathbb{R}$ be integrable, and let $t_1 \in J$, then the particular solution of the nonhomogeneous linear differential equation

$$f(t) = \kappa\frac{dy(t)}{\mathrm{d}t} + \gamma y(t) \tag{26}$$

is given by

$$y_p(t) = -\frac{1}{\kappa}\int_t^{t_1} e^{\frac{\gamma}{\kappa}(r-t)}f(r)\mathrm{d}r + e^{-\frac{\gamma}{\kappa}t}H(t_1) \tag{27}$$

where

$$H(t) = \int e^{\frac{\gamma}{\kappa}t}f(t)\mathrm{d}t \tag{28}$$

Table 1. Laplace wavelet transform for basic signals.

#	$f(t)$	$\tilde{f}_{L_\zeta}(\tau, a)$
1	$u(t)$	$c\frac{a^{1-p}}{\sigma_0}$
2	$tu(t)$	$\frac{a^2}{\sigma_0^2} + \frac{a\tau}{\sigma_0}$
3	$t^2u(t)$	$a^{-p}c\left(\frac{a\tau^2}{\sigma_0} + \frac{2a^2\tau}{\sigma_0^2} + \frac{2a^3}{\sigma_0^3}\right)$
4	$e^{-\beta t}$	$c\frac{a^{1-p}e^{-\beta\tau}}{\sigma_0 + \beta a}$
5	$\sin(\omega t)$	$ca^{-p}\frac{\omega a^2\cos(\omega\tau) + a\sigma_0\sin(\omega\tau)}{a^2\omega^2 + \sigma_0^2}$
6	$\cos(\omega t)$	$ca^{-p}\frac{\sigma_0 a\cos(\omega\tau) - a^2\omega\sin(\omega\tau)}{a^2\omega^2 + \sigma_0^2}$
7	$e^{-\xi t}\cos(\omega t)$	$ca^{-p}e^{-\xi\tau}\frac{(\sigma_0 a + \xi a^2)\cos(\omega\tau) - a^2\omega\sin(\omega\tau)}{a^2\omega^2 + (\sigma_0 + a\xi)^2}$
8	$e^{-\xi t}\sin(\omega t)$	$ca^{-p}e^{-\xi\tau}\frac{a^2\omega\cos(\omega\tau) + (\sigma_0 a + \xi a^2)\sin(\omega\tau)}{a^2\omega^2 + (\sigma_0 + a\xi)^2}$

Moreover, if $f(t)$ is exponentially bounded, such that $|f(t)| \leq |k.e^{\alpha t}| < |k.e^{|\frac{\gamma}{\kappa}|t}| \ \forall t \in J$, and if $\frac{\gamma}{\kappa} < 0$, then as $t_1 \to \infty$, $H(t_1) \to 0$ and the particular solution of equation (26) is given by

$$y_p(t) = -\frac{1}{\kappa}\int_t^{\infty} e^{\frac{\gamma}{\kappa}(r-t)} f(r)\mathrm{d}r \tag{29}$$

Proof. Using the variation of parameters method, the particular solution of equation (26) is given by the indefinite integral

$$y_p(t) = \frac{e^{\frac{\gamma}{\kappa}t}}{\kappa}\int e^{\frac{\gamma}{\kappa}t} f(t)\mathrm{d}t \tag{30}$$

By the fundamental theorem of calculus, the indefinite integral in equation (30) can be written in terms of a definite integral and the function H shown in equation (28) as

$$\int e^{\frac{\gamma}{\kappa}t} f(t)\mathrm{d}t = \int_{t_1}^{t} e^{\frac{\gamma}{\kappa}t} f(t)\mathrm{d}r + H(t_1) \tag{31}$$

Substituting equation (31) in equation (30) and switching the integral limits yields

$$y_p(t) = \frac{e^{\frac{\gamma}{\kappa}t}}{\kappa}\left(-\int_t^{t_1} e^{\frac{\gamma}{\kappa}t} f(t)\mathrm{d}r + H(t_1)\right) \tag{32}$$

which is equivalent to equation (27).

Now, suppose that $|f(t)| \leq |k.e^{\alpha t}| < |k.e^{|\frac{\gamma}{\kappa}|t}| \ \forall t \in J$ and $\frac{\gamma}{\kappa} < 0$, then

$$|H(t)| \leq \left|\int k e^{\frac{\gamma}{\kappa}t} e^{\alpha t}\mathrm{d}t\right| = \left|\frac{k e^{(\frac{\gamma}{\kappa}+\alpha)t}}{\frac{\gamma}{\kappa}+\alpha}\right| \quad \forall t \in J \tag{33}$$

since $\frac{\gamma}{\kappa} < 0$ and $|\frac{\gamma}{\kappa}| > \alpha$, then as $t \to \infty$

$$\left|\frac{k e^{(\frac{\gamma}{\kappa}+\alpha)t}}{\frac{\gamma}{\kappa}+\alpha}\right| \to 0$$

so $H(\infty) = 0$ and equation (29) follows. ■

To show that the LWT is the particular solution of the differential equation in equation (22) substitute

$$\kappa = -(1-\zeta^2)a^p$$
$$\gamma = a^{p-1}\left(j(1-\zeta^2) + \zeta\sqrt{1-\zeta^2}\right)$$

$t = \tau$, and $t_1 = \infty$ in equation (29) to obtain

$$y_p(\tau) = \tilde{f}_{L_\zeta}(\tau, a) = \left(\frac{a^{-p}}{1-\zeta^2}\right)\int_\tau^{\infty} e^{\left(\frac{-\zeta}{\sqrt{1-\zeta^2}}+j\right)\left(\frac{t-\tau}{a}\right)} f(t)\mathrm{d}t \tag{34}$$

The result obtained in Theorem 3.3, can be extended to second-and higher-order LTI systems, by following the same technique. It can be shown that the SOULTI wavelet transform (Abuhamdia et al., 2016) is the particular solution to an LTI second-order system. The proof is provided in the Appendix.

When the result is generalized to systems of first-order differential equations, instead of a scalar wavelet function, we have a tensor of wavelets or wavelet tensor.

4. LWT of elementary signals and its basic properties

The Laplace wavelet transform can be evaluated for many basic signals. It inherits many properties from the Laplace transform and the SOULTI wavelet transform.

To simplify the relations obtained from evaluating the LWT, we will denote the constant value $\zeta/\sqrt{1-\zeta^2} - j$ by σ_0, so σ is now given by

$$\sigma = \frac{\sigma_0}{a} \tag{35}$$

and the LWT definition becomes

$$\tilde{f}_{L_\zeta}(\tau, \sigma) = c a^{-p}\int_\tau^{\infty} e^{-\frac{\sigma_0}{a}(t-\tau)} f(t)\mathrm{d}t \tag{36}$$

Using equation (36), the LWT for many basic signals is evaluated and shown in Table 1. Now, we provide two important lemmas that link the LWT of the derivative/integral of the signal to the LWT of the signal itself.

4.1. Lemma: Laplace wavelet transform of derivatives

Let $J \subset (a, \infty) \subset \mathbb{R}$, and let $x(t) : J \to \mathbb{R}$ be differentiable and exponentially bounded as defined in Theorem 3.2, and let the LWT of $x(t)$ be given by equation (11), then the LWT wavelet transform of $\dot{x}(t)$ is given by

$$\mathcal{W}_{L_\zeta}\{\dot{x}(t)\}(\tau, a) = \frac{\sigma_0}{a}\mathcal{W}_{L_\zeta}\{x(t)\} - a^{-p} c x(\tau) \tag{37}$$

Proof. Direct evaluation of the LWT of $\dot{x}(t)$ by the integration by parts gives

$$\mathcal{W}_{L_\zeta}\{\dot{x}(t)\}(\tau, a) = c\, a^{-p}\left[x(t)e^{-\sigma(t-\tau)}\Big|_\tau^{\infty} + \sigma\int_\tau^{\infty} x(t)e^{-\sigma(t-\tau)}\mathrm{d}t\right] \tag{38}$$

The second term on the right side of equation (38) is the LWT of $\frac{\sigma\, x(t))}{(c a^{-p})}$. After evaluating the first term, equation (38) can be written as

$$\mathcal{W}_{L_\zeta}\{\dot{x}(t)\}(\tau, a) = c\, a^{-p}\left[-x(\tau) + \frac{\sigma}{c\, a^{-p}}\mathcal{W}_{L_\zeta}\{x(t)\}\right] \quad (39)$$

which is equivalent to equation (37). ■

4.2. Lemma: Laplace wavelet transform of integrals

Let $J \subset (a, \infty) \subset \mathbb{R}$, and let $x(t) : J \to \mathbb{R}$ be exponentially bounded as defined in Theorem 3.2, and the LWT of $x(t)$ be given by equation (11), then the LWT of $\chi(t)$, defined by

$$\chi(t) = X(t) - X(a) = \int_a^t x(r)\mathrm{d}r \quad (40)$$

is given by

$$\mathcal{W}_{L_\zeta}\{\dot{\chi}(t)\}(\tau, a) = \frac{c\, a\, \chi(\tau)}{\sigma_0} + \frac{a}{\sigma_0}\mathcal{W}_{L_\zeta}\{x(t)\} \quad (41)$$

Proof. Similar to Lemma 4.1, direct evaluation by integration by parts of the transformation integral leads to

$$\mathcal{W}_{L_\zeta}\{\dot{\chi}(t)\}(\tau, a) = c\, a^{-p}\left[\frac{\chi(\tau)\, e^{-\sigma(t-\tau)}}{-\sigma}\Big|_\tau^\infty + \frac{1}{\sigma}\int_\tau^\infty x(t)\, e^{-\sigma(t-\tau)}\mathrm{d}t\right] \quad (42)$$

The second term on the right side of equation (42) is the LWT of $\frac{x(t)}{c\, \sigma\, a^{-p}}$. After evaluating the first term on the right side, equation (42) becomes

$$\mathcal{W}_{L_\zeta}\{\dot{\chi}(t)\}(\tau, a) = c\, a^{-p}\left[\frac{\chi(\tau)}{\sigma} + \frac{a^{1+p}}{c\, \sigma_0}\mathcal{W}_{L_\zeta}\{x(t)\}\right] \quad (43)$$

which is identical to the formula in equation (41). ■

4.3. Region of convergence

The region of convergence of the LWT integral depends on the exponential boundedness of the signal, see Section 3.1. If $f(t)$ is exponentially bounded, then the Laplace wavelet transform is convergent in the scale region defined by

$$0 < a < \frac{\zeta}{\alpha\sqrt{1-\zeta^2}} \quad (44)$$

4.4. Time-frequency resolution

The Laplace wavelets possess some advantages over the SOULTI wavelets. The time-frequency resolution is an important quantity that tells the accuracy within which time and frequency information can be localized on the time-frequency domain or the time-scale domain, when scale and frequency can be related.

There are different ways to define the time-frequency resolution of a signal (Abuhamdia et al., 2016). However, the standard deviation based approach does not apply because of the zero-pole cancellation that leaves the Laplace wavelet a first-order filter with first-order transfer function in the frequency domain. Computing the center of mass for the magnitude function of a first order function does not converge, thus the standard deviation approach is not valid. Moreover, it has less significant meaning regarding frequency filtering and isolation.

Therefore, the systems theory based definitions are considered. In particular, we are presenting the quality factor based definition. The quality factor is the ratio of the peak response to the zero frequency response (Meirovitch, 1997). Let us start by finding the wavelet frequency at the maximum magnitude. The square of the magnitude of the Laplace wavelet in the frequency domain is given by

$$|a\Psi_{L_\zeta}(a\omega)|^2 = \frac{a^{2-2p}}{(1-\zeta^2)^4(a\omega-1)^2 + \zeta^2(1-\zeta^2)^2} \quad (45)$$

differentiating equation (45) with respect to ω and equating it to zero yields

$$\frac{d\,|a\Psi_{L_\zeta}(a\omega)|^2}{d\omega} = \frac{-a^{2-2p}(2a(1-\zeta^2)^4(a\omega-1))}{\left((1-\zeta^2)^4(a\omega-1)^2 + \zeta^2(1-\zeta^2)^2\right)^2} = 0 \quad (46)$$

which when solved for ω gives the frequency at the peak value by

$$\omega_p = \frac{1}{a} \quad (47)$$

This is a very important result since it shows that the frequency of the wavelet filter at the peak amplitude is the reciprocal of the scale. The relation is exact and the derivation did not involve any approximation. Figure 3 shows the Laplace wavelet function in the frequency domain at different scales, $a = 1, \frac{1}{2}, \ldots, \frac{1}{10}$. The figure clearly shows the exact centering of the peak value at exactly the frequency $1/a$.

Now, we can find the peak value of the filter. Substituting ω_p from equation (47) back into

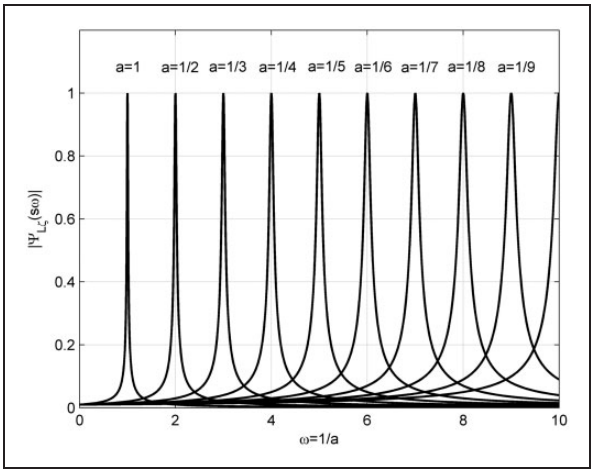

Figure 3. Laplace wavelet at different scales in the frequency domain. $\zeta = 0.01$.

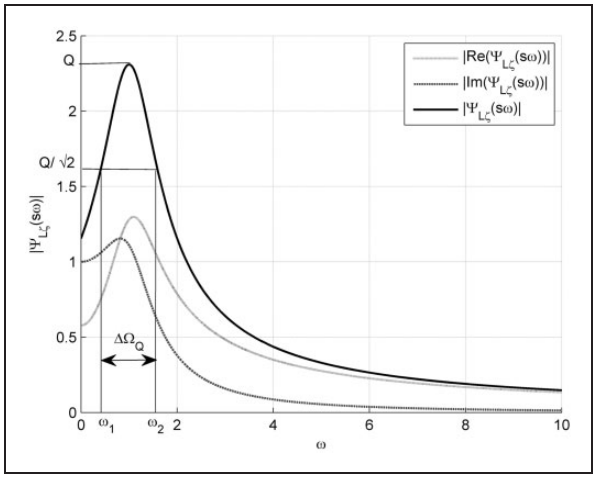

Figure 4. Laplace wavelet in the frequency domain with quality factor, half-power points, and half-power bandwidth marked. $\zeta = 0.5$.

equation (45) gives the peak magnitude as

$$Q = \frac{a^{1-p}}{\zeta\sqrt{1-\zeta^2}} \tag{48}$$

The effective frequency window, which is the half-power bandwidth, is the difference between the frequencies at half peak power, namely $|a\Psi_{L_\zeta}(a\omega)| = Q/\sqrt{2}$. Solving for the frequencies at $Q/\sqrt{2}$ and taking their difference give the frequency bandwidth as

$$\Delta\Omega_Q = \frac{2\zeta}{\sqrt{1-\zeta^2}}\omega_p \tag{49}$$

It is important to note that the $\Delta\Omega_Q$ bandwidth window of the Laplace wavelet is symmetric about the peak frequency, that is

$$\omega|_{\frac{Q}{\sqrt{2}}} = \omega_p \pm \frac{\zeta}{\sqrt{1-\zeta^2}}\omega_p \tag{50}$$

Figure 4 shows the Laplace wavelet with the half-power bandwidth, as explained in the previous analysis.

The effective time window depends on the exponential decay part of the Laplace wavelet function. Therefore, the time window based on the 2% settling time will be given by

$$\Delta T_{2\,\%} \simeq \frac{4a\sqrt{1-\zeta^2}}{\zeta} \tag{51}$$

The time-frequency resolution, which is the product of the frequency resolution and the time resolution, becomes

$$\mu = \Delta\Omega_Q.\Delta T_{2\,\%} = \frac{2\zeta}{\sqrt{1-\zeta^2}}\omega_p.\frac{4a\sqrt{1-\zeta^2}}{\zeta} = 8 \tag{52}$$

which is equal to the result obtained for the SOULTI wavelet (Abuhamdia et al., 2016). However, the derivation of the frequency bandwidth in the SOULTI case involved some approximation, while the formula is exact in the case of the Laplace wavelet. It is important to note that a 2% settling time is a too conservative limit for the time window, which can be shortened to 5% or 10% settling times.

The Laplace wavelet can be normalized by its frequency response peak value, Q, to make the peak value equal to unity at all values of ζ; thus, the normalized Laplace wavelet becomes

$$\bar{\psi}_{L_\zeta}(\tau, a) = \left(\frac{\zeta}{a\sqrt{1-\zeta^2}}\right) e^{\left(\frac{-\zeta}{\sqrt{1-\zeta^2}}+j\right)\left(\frac{t-\tau}{a}\right)} u(t-\tau) \tag{53}$$

The previous analysis shows improvement over the properties of the real SOULTI wavelet. Figure 4 shows the Laplace wavelet with both the real and the imaginary components in the frequency domain. The imaginary component represents the SOULTI wavelet, and it is clear that the Laplace peak value is centered between the real and imaginary components' peaks. As a result, the Laplace wavelet is expected to give better frequency identification and detect more precisely the change in frequencies.

5. LWT applications

The LWT has attractive potential for applications in signal processing of vibratory systems and modal parameters identification. As shown in the previous section, the Laplace wavelet has better controlled frequency bandwidth, precisely centered and controlled

filter over the desired frequencies, and good time-frequency resolution.

As a simple start for testing the capabilities of the LWT, we are processing chirps of different orders with some constant harmonics. Then, a simple example on mode separation of a three-degree-of-freedom (DOF) linear mass-spring system is presented.

5.1. Time-varying frequency identification

The Laplace wavelet can be controlled precisely to detect frequency change over time and for any frequency range. In this example, we are processing a signal consisting of quadratic chirp mixed with noise and constant harmonics at 135 Hz and 350 Hz. The analyzed signal is given by

$$S(t) = \cos\left(\frac{200\pi}{3}t^3 + 200\pi t\right) + 2\sin(270\pi t) + \sin(700\pi t) + n(t) \tag{54}$$

where $n(t)$ is a white noise component. The signal to noise ratio (SNR) of $S(t)$ is 15 dB. Figure 5 shows the signal $S(t)$.

Processing the signal $S(t)$ using the LWT reveals the frequency content of the signal and distinctly traces the time-varying frequency. Figure 6 shows the

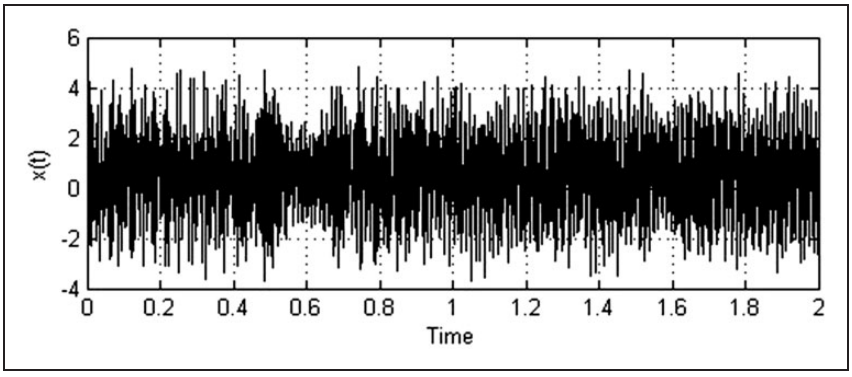

Figure 5. Quadratic chirp and two constant harmonics and white noise at SNR = 15 dB.

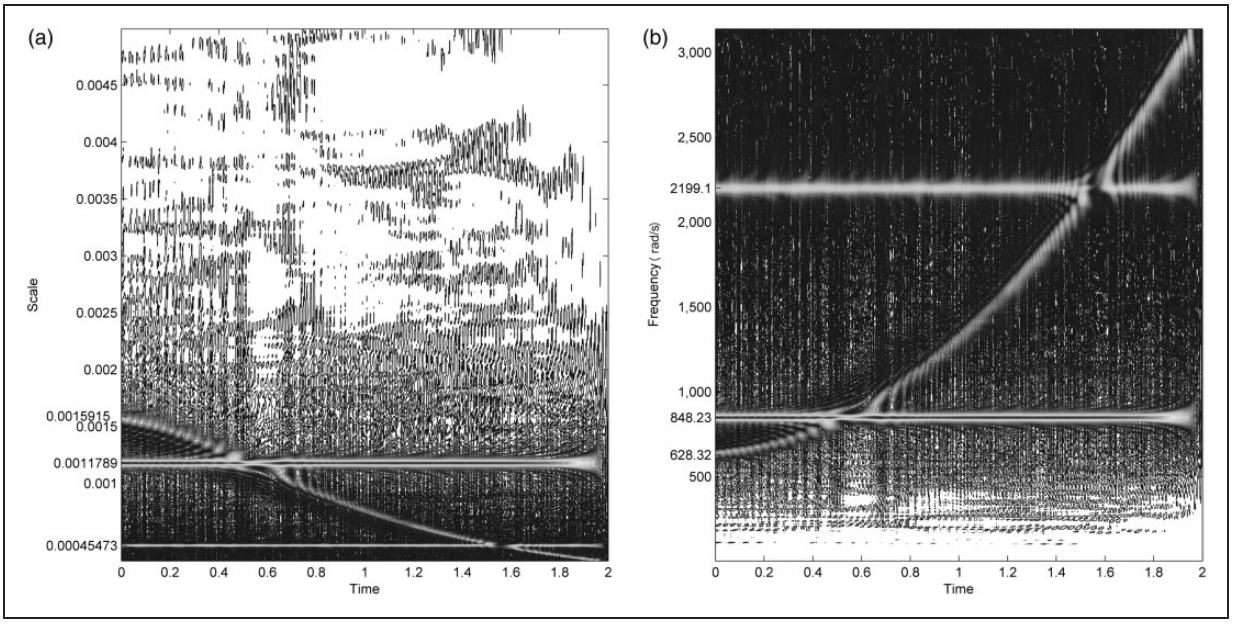

Figure 6. Laplace Wavelet Transform of $S(t)$ in equation (54): (a) time-scale contour (scalogram) (b) time-frequency countour (spectrogram). $\zeta = 0.01$.

time-scale (scalogram) and the time-frequency (spectrogram) of $S(t)$. The spectrogram precisely shows the constant harmonics at $2199.1\,\text{rad/s} = 350\,\text{Hz}$ and $848.23\,\text{rad/s} = 135\,\text{Hz}$ in addition to the quadratic chirp, which is traced along the parabola $a(t) = 200\pi t^2 + 200\pi$. The scalogram shows the reciprocal of the frequency and traces the quadratic term, which changes according to the curve $a(t) = \frac{1}{200\pi t^2 + 200\pi}$.

5.2. Analysis of 3DOF mechanical system

This section introduces a brief analysis of a 3DOF mechanical system consisting of three masses and three springs, and some friction, a schematic diagram is shown in Figure 7(a), while the actual testing bench is shown in Figure 7(b).

This example shows the capability of the Laplace wavelets in decoupling the modes of vibration.

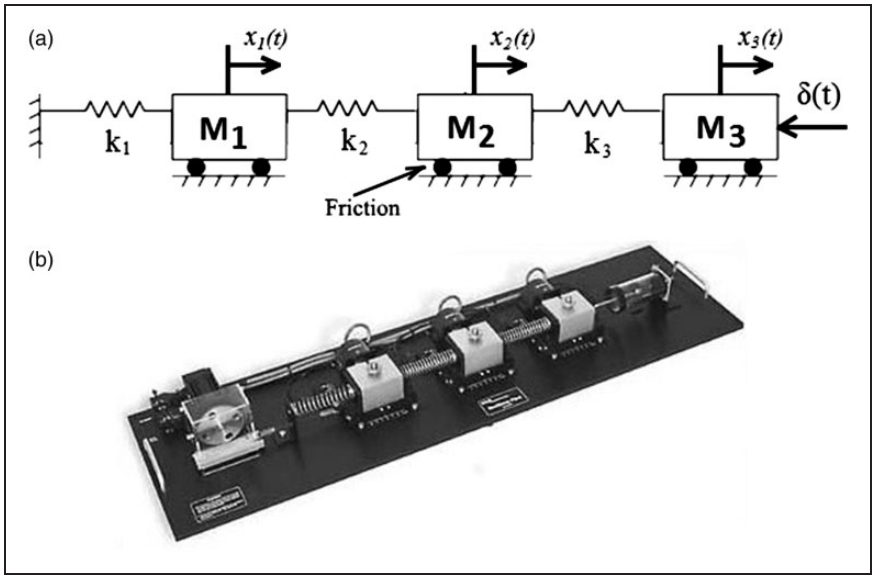

Figure 7. (a) Schematic of 3 DOF mass-spring system with friction; (b) the testing bench used in experiments.

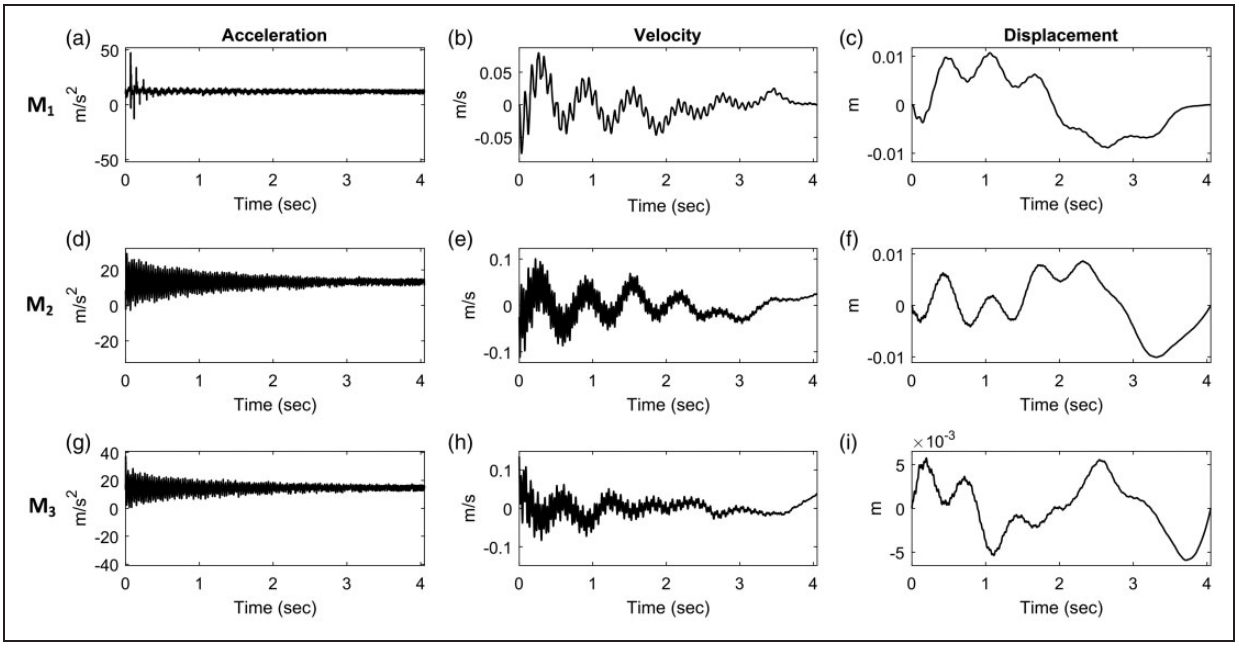

Figure 8. The response acceleration (left column), velocity (center column), and displacement (right column) for mass M_1 (top row), M_2 (middle row), and M_3 (bottom row).

The analysis here can be considered as an introduction or a first step in system identification. The classical methods of system identification behave well with linear systems, see Juang (1994); however, the LWT provides direct information and shortcuts some steps, so one can directly estimate the frequencies and the mode-shapes, and then the damping. Though we are confident of this system linearity, this confidence is not usually available with other systems, so one of the advantages that can be attained by applying the LWT is confirming or negating the LTI behavior of systems through revealing the change of natural frequencies with respect to time. LTI systems have constant natural frequencies, while nonlinear systems and time-variant systems have time-variant oscillatory frequencies.

5.2.1. Experiment and measurement system description. An impulse test was done on the three-mass test system shown in Figure 7(b). The test was performed on the system using a test hammer with a rubber head. The impulse was applied to mass M_3 as shown in Figure 7(a), then the acceleration of each mass was recorded at a sampling rate of 500 Hz using NI-6321 data acquisition card from National Instruments with LabView-2015 software. The software ran on a laptop computer with 2.4 GHz i7 dual-core processor and Windows-10 operating system. The acceleration was measured using single-axis PCB accelerometers of 10 mv/g nominal sensitivity. The accelerometers were calibrated before testing and the accurate sensitivities were used in the data conversion.

The acceleration signal can be used after filtration and detrending in the analysis, but since the acceleration signal amplifies the high frequency modes and reduces the SNR of the low frequency modes, we will obtain the velocities and the displacements for the analysis as well. The velocities and the displacements are obtained by integrating the acceleration. Figure 8 shows the acceleration, velocity, and displacement of the three masses, M_1, M_2, and M_3. Figure 8 also

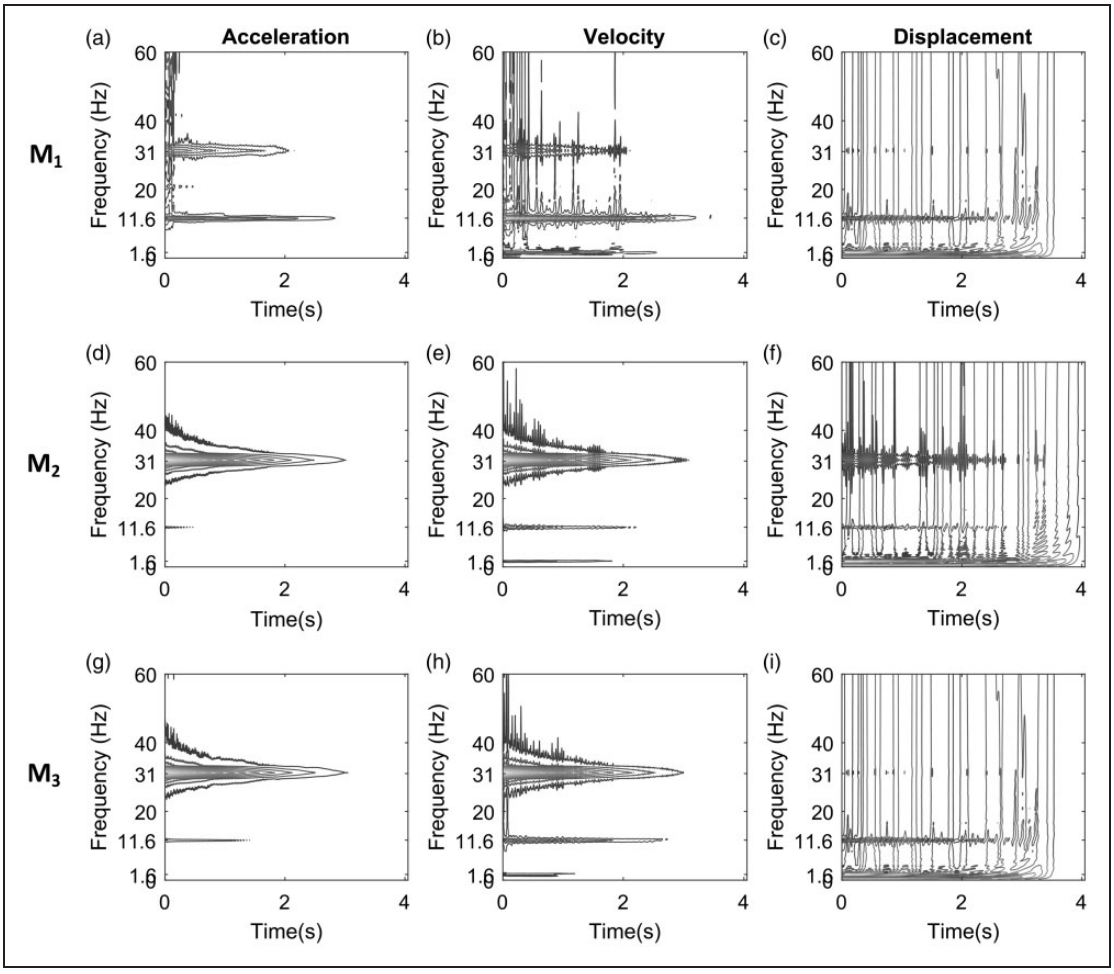

Figure 9. Spectrogram contour of the LWT, with $\zeta = 0.01$, of acceleration (left column), velocity (center column), and displacement (right column), and of M_1 (top row), M_2 (middle row), and M_3 (bottom row). The contour is plotted at 15 contour lines.

shows a constant bias in the acceleration measurement, which is typical of accelerometers due to gravity and angular inclinations. Before the velocities and the displacements were obtained, the measured acceleration signals were detrended, and the trends were largely reduced. However, the remaining trending error accrues by integration, so the trending error propagation into the displacement is the largest, see Figures 8(c), 8(f), and 8(i).

5.2.2. Time-frequency analysis by the Laplace wavelets. The LWT, with $\zeta = 0.01$, was applied to the acceleration, velocity, and displacement of the three masses. Figure 9 shows the response spectrograms of the masses $M1$, M_2, and M_3.

By examining the LWT spectrograms of the acceleration in Figure 9, we only find two ridges extending at two constant frequencies, 11.6 Hz and 31 Hz. Each ridge is centered about a modal frequency, and we see that the ridge at $f = 31$ Hz is larger, which signifies that the dominant frequency in the acceleration signal for all three masses is the highest frequency. The wavelet transforms evaluated along these ridges are called skeletons. By comparing the spectrograms of the acceleration with those of velocity, we notice a third ridge at a frequency of 1.6 Hz, which may appear on the acceleration spectrogram if the number of contour lines is increased. On the other hand, the spectrograms of the displacement of M_1 and M_3 show weak traces of the 31 Hz ridge line and clear ridges of the two lowest frequencies.

These results coincide with the results obtained from the spectrum of the nine response signals shown in Figure 10. We can identify peaks at 1.6 Hz, 11.6 Hz, and 31 Hz. However, the spectrum shows some peaks at 0.3 Hz, in Figures 10(a), (d), (e), (g), (h), and (i). The

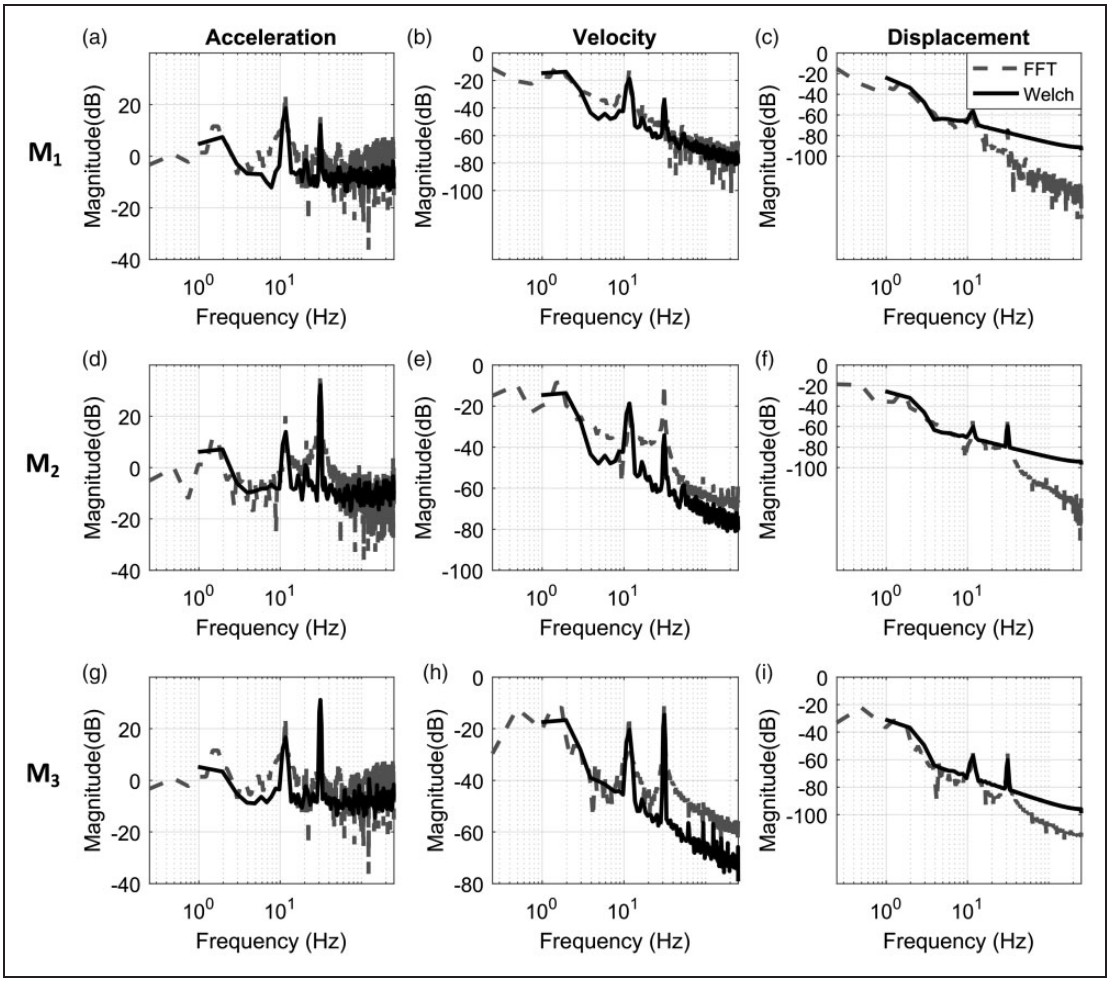

Figure 10. Spectrum on semi-log scale of the acceleration (left column), velocity (middle column), and displacement (right column) for M_1 (top row), M_2 (middle row), and M_3 (bottom row).

best results can be obtained from the LWT spectrogram of the velocities. They give three distinct ridges as shown in Figure 9(b), (e), and (h).

The LWT gives similar and relatively better result than most harmonic wavelets. To validate the LWT results and compare its advantages with the other wavelets, the spectrograms using the analytic Morse (Lilly and Olhede, 2012) and the Morlet wavelets (Morlet et al., 1982) in addition to the short time Fourier transform (STFT) spectrograms were computed for the response signals.

The continuous wavelet transform was computed in this example. The LWT was computed by discretizing the integration in equation (6) as

$$\tilde{f}_{L_\zeta}(n,m) = \left(\frac{m^{-p}}{1-\zeta^2}\right) \sum_{i=n}^{N} \overline{e^{\left(\frac{-\zeta}{\sqrt{1-\zeta^2}}+j\right)\left(\frac{i-n}{m}\right)\Delta t_i}} f(\Delta t_i)\Delta t_i \quad (55)$$

where n and m are the discrete time and frequency variables respectively, and Δt_i is the sampling time of the signal $f(t)$. To have an equivalent comparison, the Morlet wavelet transform is computed in a similar way using equation (55). The Morlet wavelet used is defined by (Lilly and Olhede, 2012)

$$\psi_m(t) = e^{\frac{-t^2}{2}} \cos(\omega t) \quad (56)$$

The continuous Morse wavelet transform is defined in the frequency domain as

$$\Psi(\omega) = U(\omega) b_{\beta,\gamma} \omega^{\beta} e^{-\omega^{\gamma}} \quad (57)$$

where b is a normalizing constant, $U(\omega)$ the step function, γ the symmetry parameter, and β the decay parameter. The transform was computed using the package developed by Lilly (2016). The Morse wavelets family employed in the analysis has a symmetry

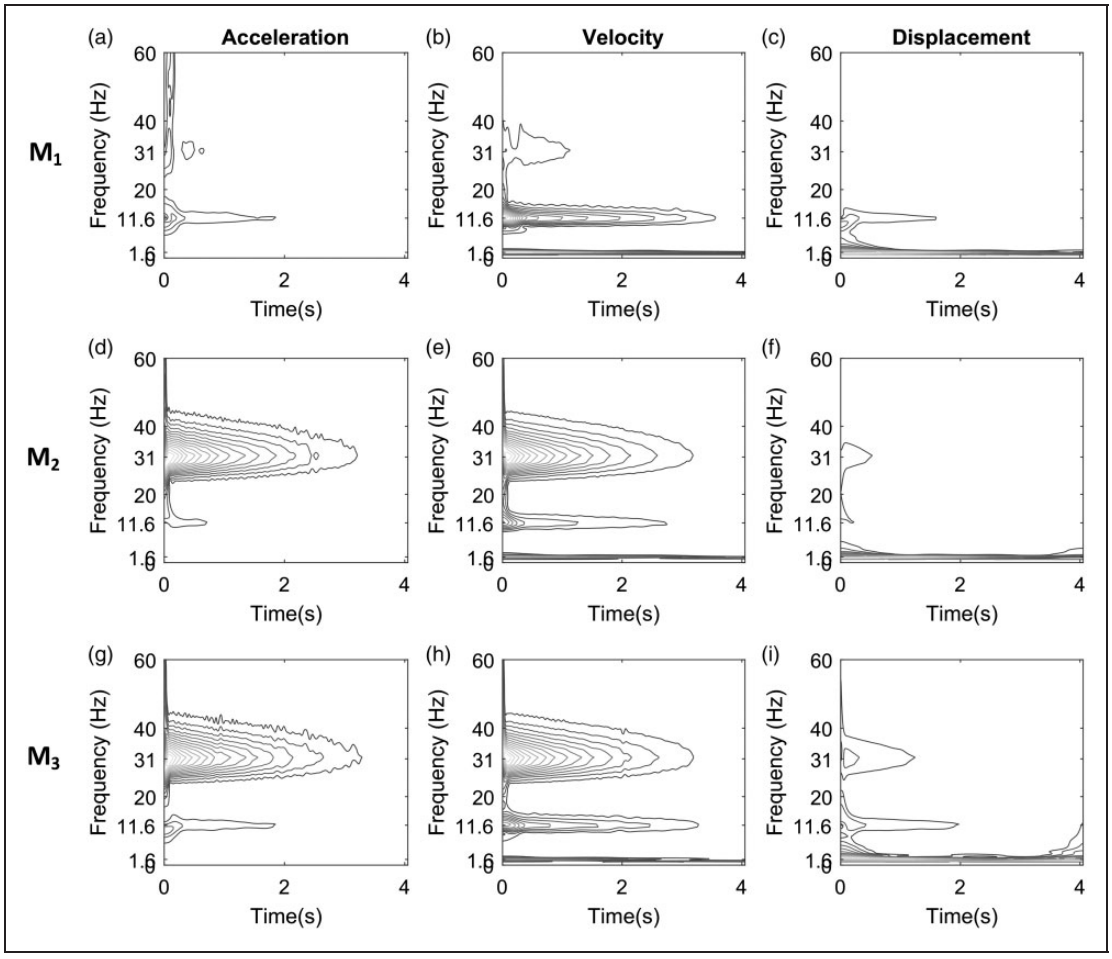

Figure 11. Spectrogram contour of the Morse wavelet transform of acceleration (left column), velocity (center column), and displacement (right column), for M_1 (top row), M_2 (middle row), and M_3 (bottom row). The contour is plotted at 15 contour lines.

parameter value $\gamma = 3$ and time-bandwidth product $\sqrt{\beta\gamma} = 60$. Figure 11 shows the Morse wavelet spectrograms of the acceleration, velocity, and displacement of the three masses. The results are similar to the LWT results, but the Morse wavelets ridges are wider, and the ridges of the displacement analysis are wider, shorter, and less visible than the LWT ridges.

The Morlet wavelet is one of the standard wavelets for time-frequency analysis. Figure 12 shows the Morlet wavelet spectrograms of the responses. The results are less crisp and do not resolve all the frequencies in the response, especially for the displacement response. Moreover, unexpected ridges at frequencies different than the modal frequency are clear and numerous, see Figure 12(a), (g), and (h).

The last comparison is made with the STFT, which is the classic method for obtaining an evolutionary spectrum or spectrogram in vibration analysis. Figure 13 presents the STFT spectrograms of the response signals. The spectrograms are narrow and extend accurately along the modal frequencies in some spectrograms, but they only reveal the lowest modal frequency in the displacement signal. In addition, the acceleration spectrograms for the masses M_2 and M_3 do not show any ridge at the lowest modal frequency. Conversely, the acceleration spectrogram of mass M_1 shows four ridges, and we notice an unexpected ridge around 20 Hz, which is not a modal frequency of the system. The clearest results are those from the velocity; however, the STFT suffers from data cuts from start and end of signals equal to the analysis window length. The analysis window used in the STFT is 1 second of length, and notice a 1 second cut from both ends of the spectrograms time axis.

5.2.3. Modes decomposition. By using the fast Fourier transform (FFT) spectrum as a reference, we find that the ridges of the LWT spectrograms extend along the three modal frequencies. In the following analysis, we employ the velocity response of the three masses

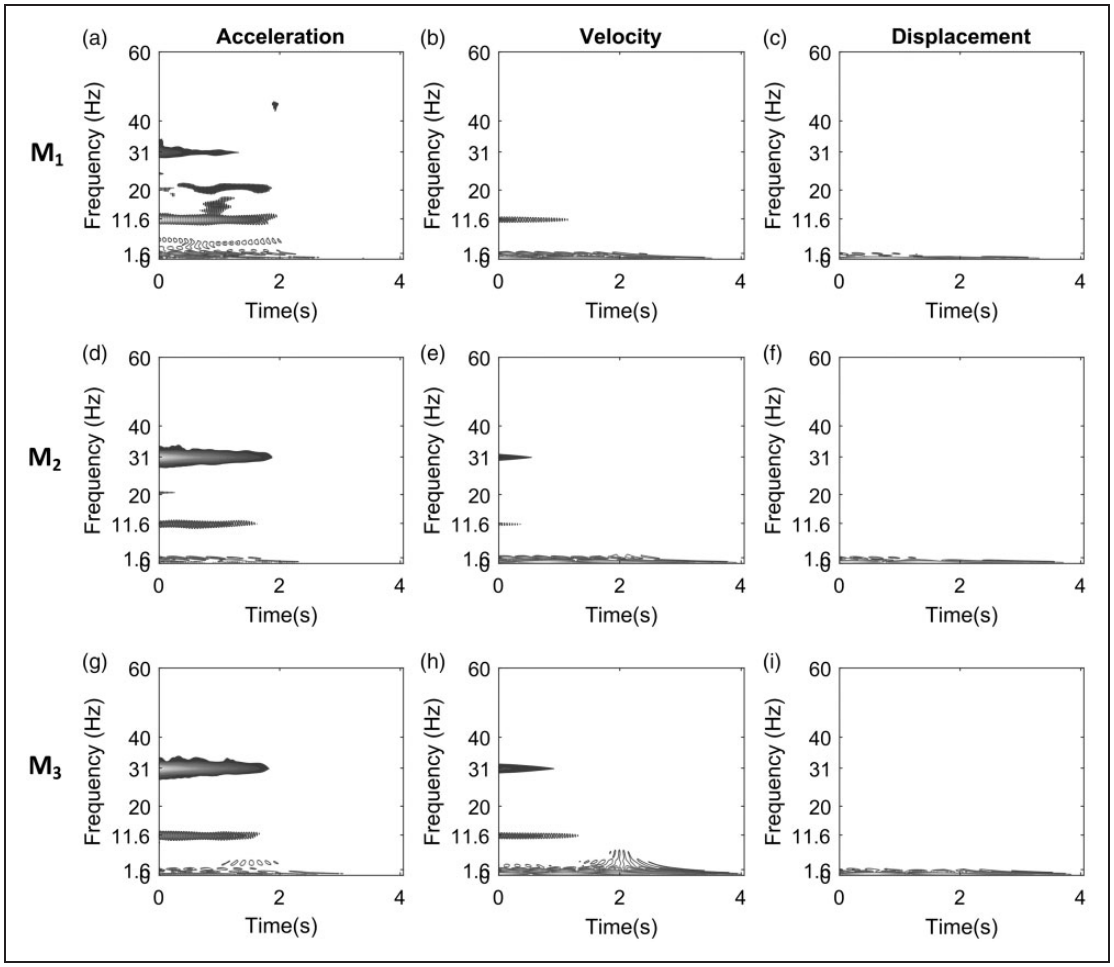

Figure 12. Spectrogram contour of the Morlet wavelet transform of acceleration (left column), velocity (center column), and displacement (right column), for M_1 (top row), M_2 (middle row), and M_3 (bottom row). The contour is plotted at 15 contour lines.

because its spectrograms offer clear distinct ridges at these modal frequencies. Since the system possesses only three major frequencies that are constant with respect to time, this gives strong indication that the system behaves linearly in the range of operation that has been tested. Therefore, the mode i of the response is given by

$$x_i(t) = \sum_{k=1}^{3} e^{\xi_k \omega_k t}\left(c_{ki_1}\cos(\omega_k t) + c_{ki_2}\sin(\omega_k t)\right) \tag{58}$$

From Table 1, the LWT of the response in equation (58) is given by

$$\mathcal{W}_{L_\zeta}\{x_i(t)\} = \sum_{k=1}^{3} e^{-\xi_k \tau} \times \left(\frac{c_{ki_1}\left((\sigma_0 a + \xi_k a^2)\cos(\omega_k \tau) - a^2\omega_k \sin(\omega_k \tau)\right)}{a^2\omega_k^2 + (\sigma_0 + a\xi_k)^2} + \frac{c_{ki_2}\left(a^2\omega_k \cos(\omega_k \tau) + (\sigma_0 a + \xi_k a^2)\sin(\omega_k \tau)\right)}{a^2\omega_k^2 + (\sigma_0 + a\xi_k)^2}\right) \tag{59}$$

which shows that the LWT preserves the frequency and the exponential decay of the original signal. The result in equation (59) is a complex valued function. With some algebraic manipulations, it can be shown that the norm of equation (59), which is used to plot the spectrograms is given by

$$|\mathcal{W}_{L_\zeta}\{x_i(t)\}| = \sum_{k=1}^{3} e^{-\xi_k \omega_k \tau}\left(c_{ki_1}\sqrt{\frac{\frac{a^4\omega_k^2}{2} + \frac{h}{2} + \sqrt{\left(\frac{a^4\omega_k^2 - h}{2}\right)^2 + \left((aD + a^2\xi_k)a^2\omega\right)^2}\sin(2\omega_k\tau + \phi_k)}{\left(a^2(\omega_k^2 + \xi_k^2) + 2a\xi_k\right)^2 + 4(D + a\xi)^2}} + c_{ki_2}\sqrt{\frac{\frac{a^4\omega_k^2}{2} + \frac{h}{2} + \sqrt{\left(\frac{a^4\omega_k^2 - h}{2}\right)^2 + \left((ax + a^2\xi_k)a^2\omega_k\right)^2}\cos(2\omega_k\tau + \phi_k)}{\left(a^2(\omega_k^2 + \xi_k^2) + 2a\xi_k\right)^2 + 4(D + a\xi_k)^2}}\right) \tag{60}$$

where $h = ((aD + a^2\xi)^2 + a^2)$ and $D = \frac{\zeta}{\sqrt{1-\zeta^2}}$. The terms under the radical, in equation (60), show that the norm adds a constant gain multiplied by an exponential term. Note that the sinusoidal terms' argument has $2\omega_k\tau$ and $\cos(2\omega_k\tau + \phi) = 2\cos^2(\omega_k\tau + \phi/2) - 1$. Therefore, we would expect the transform to resemble decaying oscillations added to an exponentially decaying function.

Figure 14 shows skeletons at the spectrogram's ridges of the displacement, which are the skeletons along the ridges in Figure 9(c). Each skeleton line decays to zero, and each carries a different major frequency. The skeleton lines show offset from the zero axis because they represent the norm of the transform which is greater than or equal to zero, and this adds an offset to the results as shown by equation (60). The skeletons represent the LWT at the scales corresponding to the central frequencies of the ridges. Notice that the first mode $f_1 = 1.6$ Hz is the most dominant mode in the displacement spectrograms. Figure 14(b) and (c) show that its effect propagates to the second and third modes.

Figures 15 to 17 show the skeletons at the modal ridges of the velocity spectrograms, $\dot{x}_1(t)$, $\dot{x}_2(t)$, and $\dot{x}_3$, and they compare among Laplace, Morlet, and the Morse wavelets in addition to the STFT. All the lines are normalized, so the maximum value of each is 1.

The LWT skeleton lines show the most uniform decay that closely looks like an exponential decay. This agrees with the results in equations (59) and (60). The closest lines to the LWT skeleton lines are the STFT lines. Each LWT skeleton line carries a single major frequency. The oscillation frequencies, carried by the LWT skeleton lines in Figure 15(a), (b), and (c) are 1.6 Hz, 11.6 Hz, and 31 Hz respectively, which is predicted by equation (59). This is not the case with the other wavelets and the STFT. The STFT skeleton is almost not oscillating and cut from both ends, so it does not reveal the behavior at the beginning and end of the signal. The Morse wavelet skeleton is not uniform and the least regular in shape. In addition, the Morlet wavelet skeletons carry scaled frequencies by approximately a factor of 1/5. If the sinusoid in equation (56) has a frequency of ω, then the Morlet wavelet

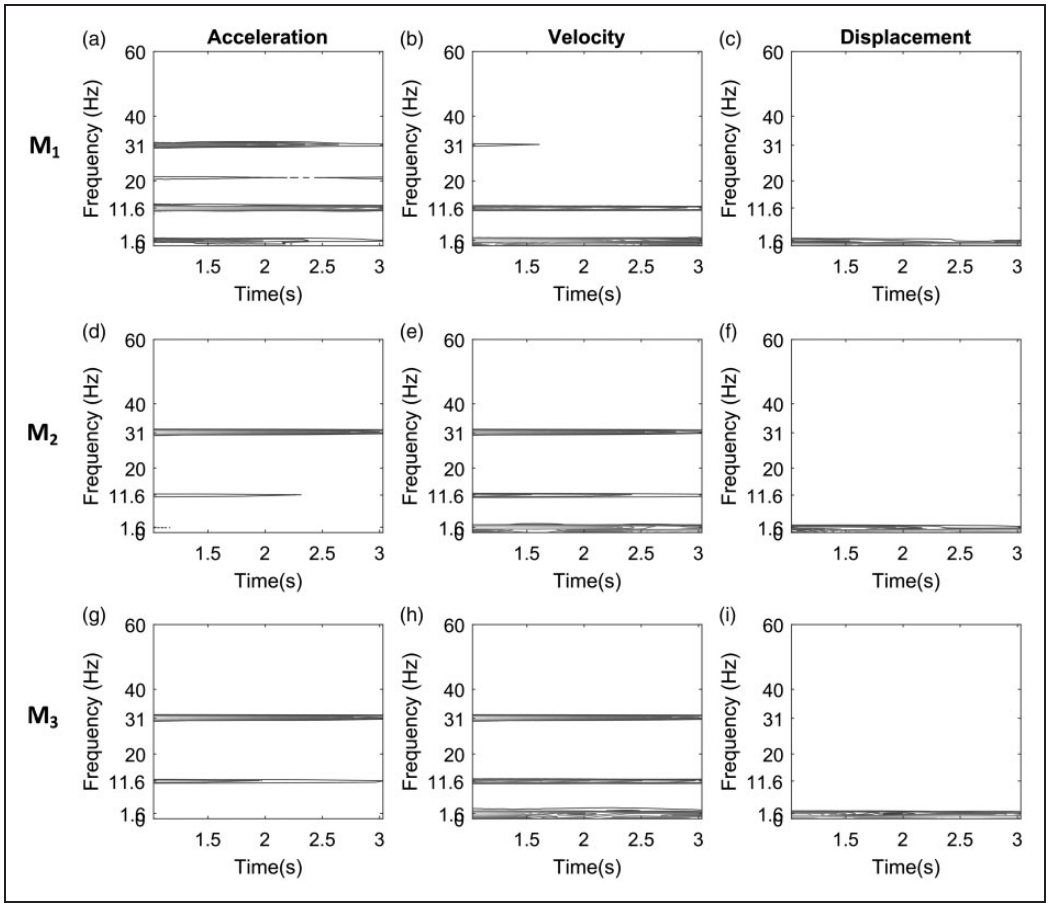

Figure 13. Spectrograms contours of the STFT of acceleration (left column), velocity (center column), and displacement (right column), for M_1 (top row), M_2 (middle row), and M_3 (bottom row). The contour is plotted at 15 contour lines.

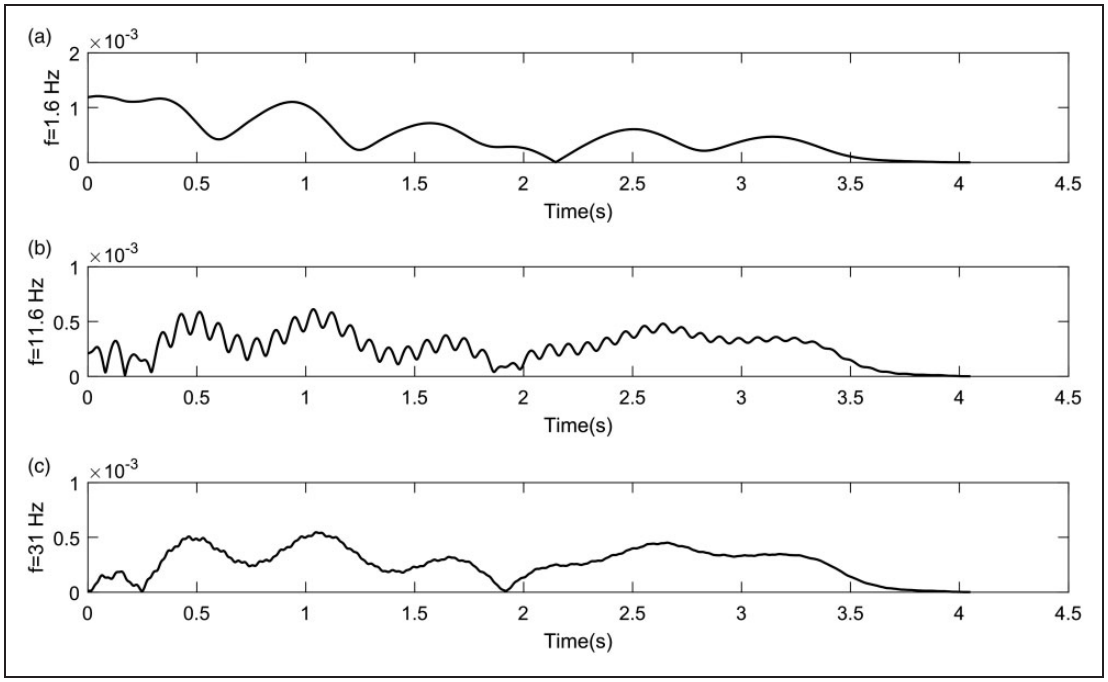

Figure 14. LWT mode decomposition of $x_1(t)$. Skeleton lines at the modal ridges from mass M_1 displacement spectrograms shown in Figures 9 and 11 to 13.

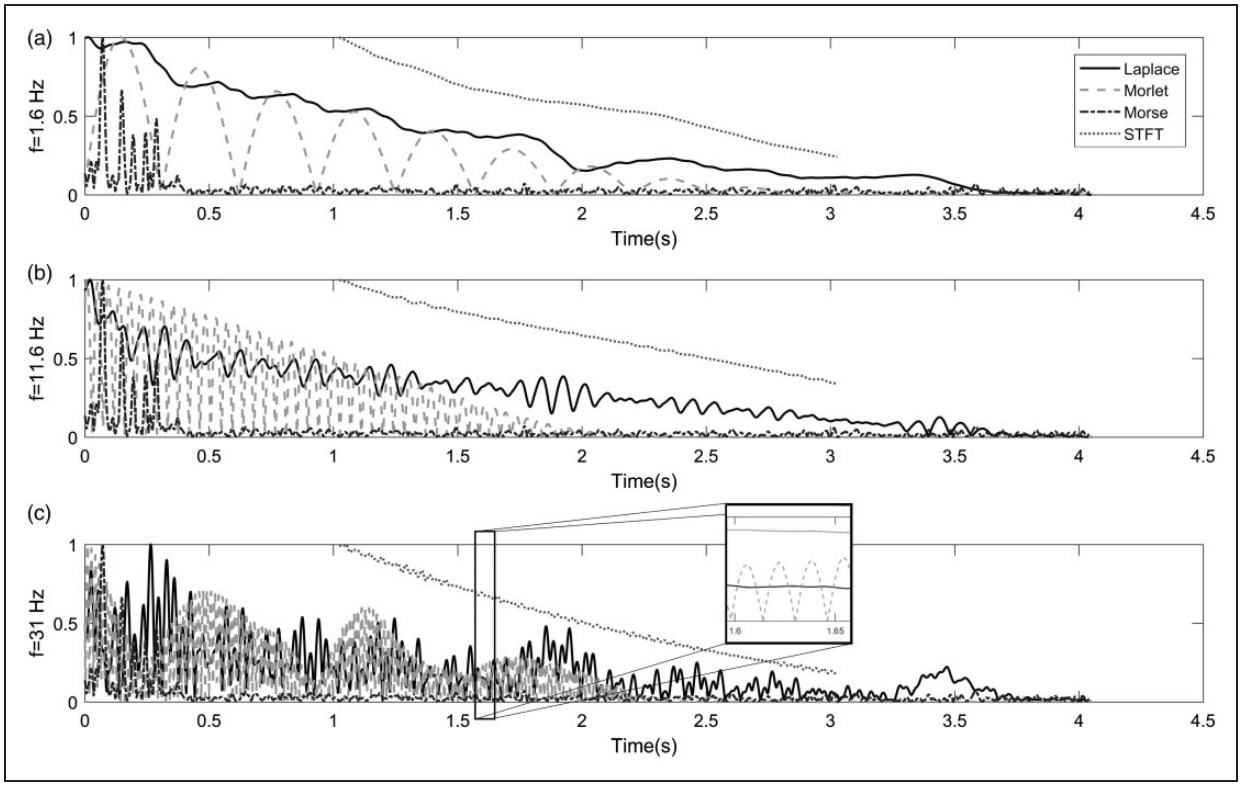

Figure 15. Skeleton lines at the modal ridges from the velocity spectrograms of mass M_1 shown in Figures 9 and 11 to 13. (a) 1.6 Hz skeleton; (b) 11.6 Hz skeleton; (c) 31 Hz skeleton.

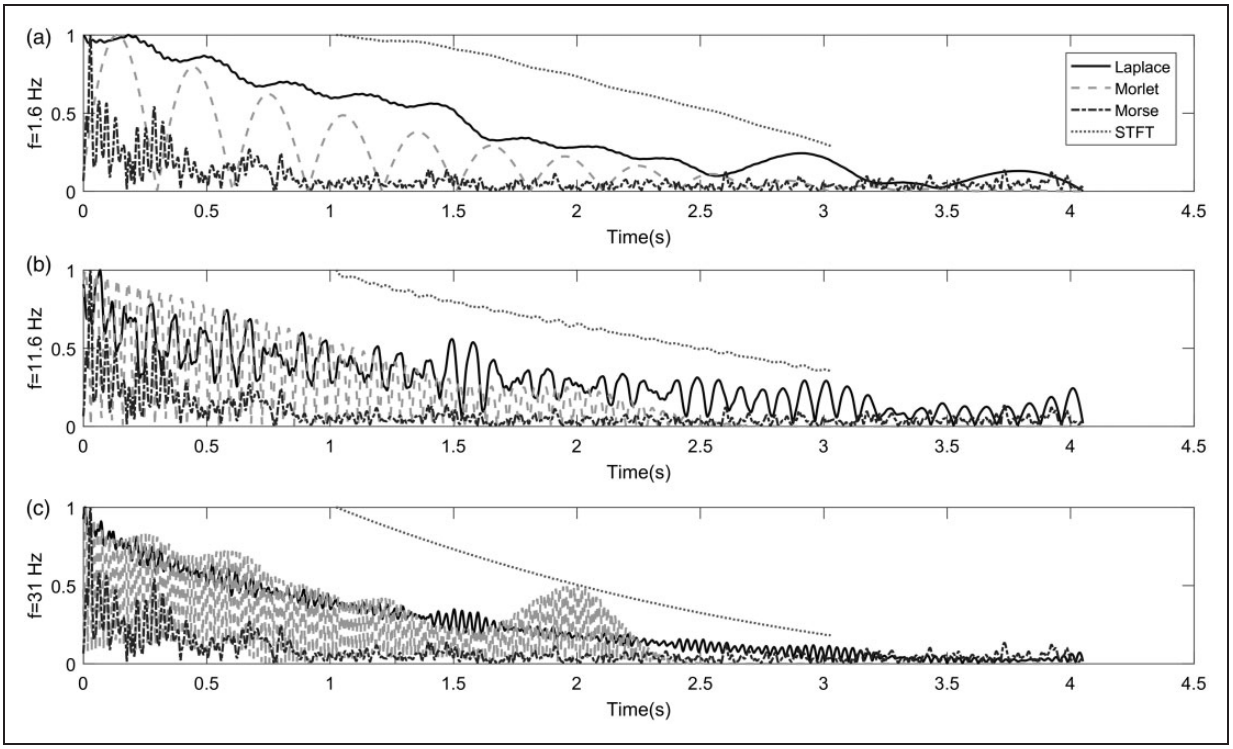

Figure 16. Skeleton lines at the modal ridges of mass M_2 velocity spectrograms shown in Figures 9 and 11 to 13. (a) 1.6 Hz skeleton; (b) 11.6 Hz skeleton; (c) 31 Hz skeleton, notice the enlarged section.

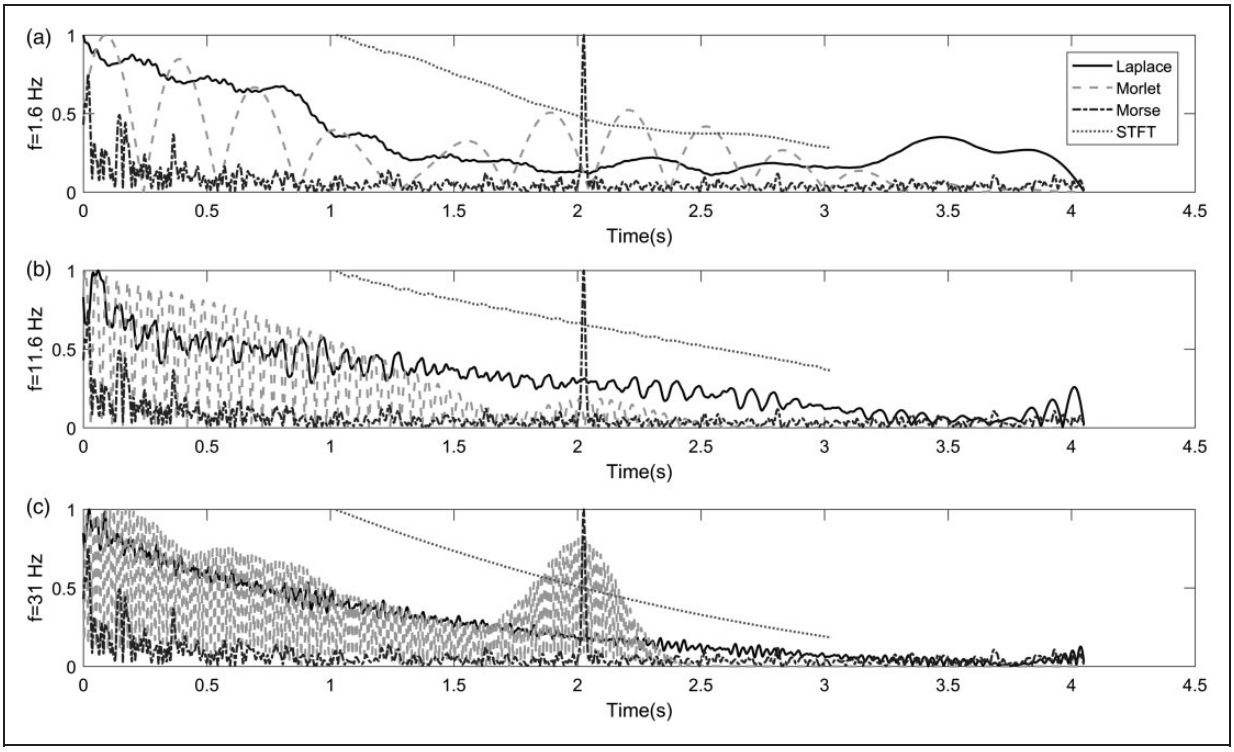

Figure 17. Skeleton lines at the modal ridges of mass M_3 velocity spectrograms shown in Figures 9 and 11 to 13. (a) 1.6 Hz skeleton; (b) 11.6 Hz skeleton; (c) 31 Hz skeleton.

filter is centered at frequency $\omega_{\text{peak}} \approx \omega/5$ in the frequency domain. Moreover, the decay shape significantly deviates from the exponential decay at many instances.

The previous analysis shows that the response signal of the LTI-MDOF (multi-degree-of-freedom) system can be decomposed using the LWT into N components, where N is equal to the number of DOF. Moreover, each component carries the property of a single mode of the response modes.

6. Conclusion

The previous presentation introduces the theory of the Laplace families of wavelets. Each family is linked or determined by a distinct ζ. The Laplace wavelet is not orthogonal or biorthogonal, but for every function in the family, we can find an orthogonal function given by equation (5). Furthermore, its wavelet transform can be reversed, and it can be evaluated and give close-form formulas for most basic signals. Two methods for inverting the LWT were derived; one is a double integration formula, and the second is a differential equation. Also, the study showed that the LWT is the particular solution of the reconstruction differential equation. This result supports the notion of treating wavelets as an output of a natural system and looking at systems' responses as potential wavelets.

The LWT inherits many properties from the Laplace transform and gives slightly better properties than the SOULTI transform. The LWT can be evaluated for most basic signals in a similar way to the traditional Laplace transform. The LWT has effective windows of resolution that can be defined in both time and frequency. Moreover, the scale can be directly linked to frequency, which makes the switch between the time-scale and time-frequency domains easy and intuitive.

The Laplace wavelets proved to be useful in systems and vibrations analysis due to its ability to distinguish frequencies and its ease of evaluation. Moreover, it can be applied to systems described by LTI differential equations because the LWT of the derivative or integral of a signal can be inferred from the LWT of the signal. The Laplace wavelet is able to extract frequencies and provide clear spectrograms, where the instantaneous frequencies can be accurately traced. Moreover, when the LWT is applied to the response of MDOF systems, the modes of vibrations can be separated or

decoupled distinctly. Comparing the spectrograms of the LWT with the spectrograms of other wavelets and the STFT shows competitive frequency resolution of LWT, yet the advantage of the LWT is more visible in the skeletons of the modes' ridges, which preserve the exponential decay and the modal frequency.

The aforementioned theoretical and experimental results give strong hints about the potentials of the Laplace wavelets for different applications especially in dynamic systems and mechanical vibrations.

Acknowledgements

The authors would like to thank Ms. Sydney Jones and Ms. Hong Ju Kim for their editorial tips and suggestions.

Declaration of Conflicting Interests

The author(s) declared no potential conflicts of interest with respect to the research, authorship, and/or publication of this article.

Funding

The author(s) received no financial support for the research, authorship, and/or publication of this article.

References

Abuhamdia T and Taheri S (2015) Wavelets as a tool for systems analysis and control. *Journal of Vibration and Control*. Epub ahead of print 16 December 2015. DOI:1077546315620923.

Abuhamdia T, Taheri S and Burns J (2016) A new wavelet family based on second-order LTI-systems. *Journal of Vibration and Control*. Epub ahead of print 19 October 2016. DOI:1077546316674089.

Freudinger LC, Lind R and Brenner MJ (1998) Correlation filtering of modal dynamics using the Laplace wavelet. In: *International modal analysis conference*, Santa Barbara, CA. SEM, Bethel, CT, USA, vol. 2, pp.868–877.

Jezequel L and Argoul P (1986) New integral transform for linear systems identification. *Journal of Sound and Vibration* 111(2): 261–278.

Juang J-N (1994) *Applied System Identification*. Upper Saddle River, NJ, USA: Prentice Hall.

Lilly JM (2016) A data analysis package for Matlab, version 1.6.2. Available at: http://www.jmlilly.net/jmlsoft.html

Lilly JM and Olhede SC (2012) Generalized Morse wavelets as a superfamily of analytic wavelets. *IEEE Transactions on Signal Processing* 60(11): 6036–6041.

Meirovitch L (1997) *Principles and Techniques of Vibrations*. Vol. 1, Upper Saddle River, NJ: Prentice Hall.

Morlet J, Arens G, Fourgeau E, et al. (1982) Wave propagation and sampling theory-part II: Sampling theory and complex waves. *Journal of Geophysics* 47(2): 222–236.

Naylor AW and Sell GR (2000) *Linear Operator Theory in Engineering and Science*. New York: Springer Science & Business Media.

Yoshida K (1965) *Functional Analysis*. Vol. 123, 1st ed. Berlin Heidelberg, Germany: Springer-Verlag.

Appendix: Second-order LTI ODE's particular solution

The SOULTI wavelet is defined in equation (1). Let $f(t)$ be as defined in Sections 2.1 and 3.1, then the SOULTI wavelet transform of $f(t)$ is defined by the generic continuous wavelet transform

$$\mathcal{W}_\zeta\{f(t)\} = \tilde{f}_\zeta(\tau, a) = \int_\tau^\infty f(t)\psi_\zeta\Big(\frac{t-\tau}{a}\Big)dt,\ \tau \in (-\infty, \infty) \tag{61}$$

Moreover, if $f(t)$ is differentiable, then it satisfies the differential equation

$$f(t) = a^{p-1}\left[(1-\zeta^2)a^2\frac{d^2\Big(\tilde{f}_\zeta(t,a)\Big)}{dt^2} - 2\sqrt{1-\zeta^2}\zeta a\frac{d\Big(\tilde{f}_\zeta(t,a)\Big)}{dt} + \tilde{f}_\zeta(t,a)\right] \tag{62}$$

For proof, see Abuhamdia et al. (2016). Equation (62) serves as an inverse wavelet transform of $\tilde{f}_\zeta(\tau, a)$. In the following, we prove that $\tilde{f}_\zeta(\tau, a)$ is the particular solution of equation (62).

Theorem: Particular solution of second-order autonomous ODEs

Let $J \subset (a, \infty) \subset \mathbb{R}$, and let $f(t) : J \to \mathbb{R}$ be integrable and exponentially bounded, and let s_1 and s_2 be the roots of the accompanying characteristic equation of the autonomous non-homogeneous differential equation

$$f(t) = l\,\frac{d^2y(t)}{dt^2} + h\,\frac{dy(t)}{dt} + g\,y(t) \tag{63}$$

if $s_1 \neq s_2$, then the particular solution of equation (63) is given by the wavelet transform defined by

$$y_p(t) = \int_t^{t_1} \psi(r-t)f(r)\mathrm{d}r + K(t) \tag{64}$$

where $t \in J$, $K(t, t_1)$ is a function that depends on the parameters of the differential equation and t_1, and $\psi(t)$ is defined by

$$\psi(t) = \frac{e^{-s_2 t} - e^{-s_1 t}}{l(s_2 - s_1)} \tag{65}$$

Proof. The solution of the homogeneous version of equation (63) is given by

$$y_h(t) = c_1 y_1(t) + c_2 y_2(t) = c_1 e^{s_1 t} + c_2 e^{s_2 t} \tag{66}$$

where s_1 and s_2 are given by

$$s_{1,2} = \frac{-h}{2l} \pm \frac{\sqrt{h^2 - 4lg}}{2l} \tag{67}$$

whereas the particular solution $y_p(t)$ is given by

$$y_p(t) = y_2(t) \int \frac{y_1(t) f(t)}{l\, W(y_1(t), y_2(t))} \mathrm{d}t - y_1(t) \int \frac{y_2(t) f(t)}{l\, W(y_1(t), y_2(t))} \mathrm{d}t \tag{68}$$

where $W(y_1(t), y_2(t))$ is the Wronskian of $y_1(t)$ and $y_2(t)$ and is given by

$$W(y_1(t), y_2(t)) = \begin{vmatrix} y_1(t) & y_2(t) \\ y_1'(t) & y_2'(t) \end{vmatrix} = (s_2 - s_1) e^{(s_1 + s_2)t} \tag{69}$$

substituting $y_1(t)$, $y_2(t)$, and $W(y_1(t), y_2(t))$ into equation (68) and simplifying yields

$$y_p(t) = e^{s_2 t} \int \frac{e^{-s_2 t} f(t)}{l\,(s_2 - s_1)} \mathrm{d}t - e^{s_1 t} \int \frac{e^{-s_1 t} f(t)}{l\,(s_2 - s_1)} \mathrm{d}t \tag{70}$$

the indefinite integrals in equation (70) can be rewritten in the form of definite integrals, so equation (70) becomes

$$\begin{aligned} y_p(t) = {} & e^{s_1 t} \int_t^{t_1} \frac{e^{-s_1 r} f(r)}{l\,(s_2 - s_1)} \mathrm{d}r - e^{s_1 t} k_1(t_1) + e^{s_2 t} k_2(t_1) \\ & - e^{s_2 t} \int_t^{t_1} \frac{e^{-s_2 r} f(r)}{l\,(s_2 - s_1)} \mathrm{d}r \end{aligned} \tag{71}$$

where $k_1(t)$ and $k_2(t)$ are given by

$$\begin{aligned} k_1(t) &= \int \tfrac{e^{-s_1 t} f(t)}{l\,(s_2 - s_1)} \mathrm{d}t \\ k_2(t) &= \int \tfrac{e^{-s_2 t} f(t)}{l\,(s_2 - s_1)} \mathrm{d}t \end{aligned} \tag{72}$$

Collecting the terms and defining $K(t, t_1)$ as

$$K(t, t_1) = e^{s_1 t} k_1(t_1) - e^{s_2 t} k_2(t_1) \tag{73}$$

gives $y_p(t)$ as

$$y_p(t) = \int_t^{t_1} \frac{e^{-s_1(r-t)} - e^{-s_2(r-t)}}{l\,(s_2 - s_1)} f(r)\, \mathrm{d}r + K(t, t_1) \tag{74}$$

which completes the proof. ■

It is important to note that even if $s_1 = s_2$, in other words the system has repeated roots, the particular solution can still be expressed as a wavelet transform. This can be easily proved using the particular solution of a system of first-order differential equations. In the following we show that the SOULTI wavelet transform is the particular solution of equation (62).

Corollary: Particular solution of the reconstructing DE

Let $J \subset (a, \infty) \subset \mathbb{R}$, and let $f(t) : J \to \mathbb{R}$ be integrable and exponentially bounded, then there exists a and $0 < \zeta < 1$ such that the particular solution of equation (62) is given by the SOULTI wavelet transform

$$y_p(t) = \tilde{f}_\zeta(t, a) = \int_t^\infty \left(\frac{a^{-p}}{1 - \zeta^2} \right) e^{\frac{-\zeta}{\sqrt{1-\zeta^2}} \left(\frac{r-t}{a} \right)} \sin\left(\frac{r - t}{a} \right) f(r)\, \mathrm{d}r \tag{75}$$

Proof. by comparing equation (62) to equation (63) we find that the parameters of the autonomous homogeneous differential equation in equation (62) are given as follows

$$l = a^{p+1}(1 - \zeta^2) \tag{76}$$

$$h = -2a^p \zeta \sqrt{1 - \zeta^2} \tag{77}$$

$$g = a^{p-1} \tag{78}$$

substituting equation (76) into equation (74) and letting $t_1 \to \infty$ we get

$$y_p(t) = \int_t^\infty \frac{e^{\left(\frac{-\zeta}{a\sqrt{1-\zeta^2}} + i \right)(r-t)} - e^{\left(\frac{-\zeta}{a\sqrt{1-\zeta^2}} - i \right)(r-t)}}{-i2a^p(1 - \zeta^2)} f(r)\, \mathrm{d}r - K(t, \infty) \tag{79}$$

Using the Euler formula, equation (79) reads

$$y_p(t) = \int_t^{\infty} \left(\frac{a^{-p}}{1-\zeta^2}\right) e^{\frac{-\zeta}{\sqrt{1-\zeta^2}}\left(\frac{r-t}{a}\right)} \sin\left(\frac{r-t}{a}\right) f(r)\, \mathrm{d}r - K(t,\infty) \tag{80}$$

Now, we have to show that $K(t, t_1)$ vanishes as $t_1 \to \infty$. Since $f(t)$ is of exponential order, then there exists m, a, $0 < \zeta < 1$, and $\alpha > 0$ all $\in \mathbb{R}$, such that $|f(t)| \leq |me^{\alpha t}| \leq |me^{a\sqrt{1-\zeta^2}t}|\ \forall\ t \in J$. Therefore, $k_1(t)$ and $k_2(t)$ are bounded by the inequalities

$$|k_1(t)| \leq \left| \int \frac{m\, e^{\left(\frac{-\zeta}{a\sqrt{1-\zeta^2}}+i\right)t} e^{\alpha t}}{l\,(s_2 - s_1)} \mathrm{d}t \right| \quad \forall t \in J \tag{81}$$

$$|k_2(t)| \leq \left| \int \frac{m\, e^{\left(\frac{-\zeta}{a\sqrt{1-\zeta^2}}-i\right)t} e^{\alpha t}}{l\,(s_2 - s_1)} \mathrm{d}t \right| \quad \forall t \in J \tag{82}$$

after evaluating the integrals, they become

$$|k_1(t)| \leq \left| \frac{m\, e^{\left(\frac{-\zeta}{a\sqrt{1-\zeta^2}}+\alpha+i\right)t}}{l\,(s_2 - s_1)\left(\left(\frac{-\zeta}{a\sqrt{1-\zeta^2}} + \alpha + i\right)\right)} \right| \quad \forall t \in J \tag{83}$$

$$|k_2(t)| \leq \left| \frac{m\, e^{\left(\frac{-\zeta}{a\sqrt{1-\zeta^2}}+\alpha-i\right)t}}{l\,(s_2 - s_1)\left(\left(\frac{-\zeta}{a\sqrt{1-\zeta^2}} + \alpha - i\right)\right)} \right| \quad \forall t \in J \tag{84}$$

but as $t \to \infty$ both quantities on the left of inequalities 83 vanish. Therefore,

$$\lim_{t\to\infty} k_1(t) = \lim_{t\to\infty} k_2(t) = 0 \tag{85}$$

hence $K(t, \infty) = 0$ in equation (80), and we obtain equation (75). ■